Modification of sea surface temperature by chlorophyll concentration in the Atlantic upwelling systems

Olga Hernandez, Julien Jouanno, Vincent Echevin, Olivier Aumont

AGU PUBLICATIONS

JGR

Journal of Geophysical Research: Oceans

RESEARCH ARTICLE

10.1002/2016JC012330

Modification of sea surface temperature by chlorophyll concentration in the Atlantic upwelling systems

O. Hernandez[1,2], J. Jouanno[1], V. Echevin[3], and O. Aumont[3]

[1]LEGOS, Université de Toulouse, CNES, CNRS, IRD, UPS, Toulouse, France, [2]Now at Mercator-Océan, Ramonville Saint Agne, France, [3]CNRS-IRD-Sorbonne Universités, UPMC, MNHN, LOCEAN Laboratory, Paris, France

Key Points:
- Biological impact on the physics is investigated with an ocean model forced with chlorophyll-dependent penetrative solar radiation
- Chlorophyll concentrations in the eastern Tropical Atlantic cool the Benguela and Mauritania-Senegal upwelling systems by around 1°C
- The processes responsible for the observed cooling are examined using Lagrangian and Eulerian heat budgets

Correspondence to:
O. Hernandez,
olgahernand@gmail.com

Citation:
Hernandez, O., J. Jouanno, V. Echevin, and O. Aumont (2017), Modification of sea surface temperature by chlorophyll concentration in the Atlantic upwelling systems, *J. Geophys. Res. Oceans*, *122*, 5367–5389, doi:10.1002/2016JC012330.

Received 22 SEP 2016
Accepted 11 MAY 2017
Accepted article online 17 MAY 2017
Published online 4 JUL 2017

Abstract The influence of the chlorophyll on the upper Tropical Atlantic Ocean is investigated with long-term (1979–2012) regional oceanic simulations with 1/4° horizontal resolution based on the NEMO3.6 model. The model solar radiation penetration scheme depends on the chlorophyll concentration. Simulations with time and spatially varying concentrations obtained from satellite ocean color observations are compared with a simulation forced with constant chlorophyll concentration of 0.05 mg m^{-3}, representative of chlorophyll depleted waters. Results indicate that regions of the Tropical Atlantic with chlorophyll concentrations larger than in the reference simulation (i.e., [chl] $>$ 0.05 mg m^{-3}) get warmer at the surface, with the exception of the main upwelling regions where high chlorophyll concentrations are associated with a significant cooling of the sea surface ($\sim$1°C in the Benguela upwelling). The analysis of the model heat balance shows that the biological differential heating causes negative temperature anomalies in subsurface source waters prior to their upwelling at the coast. The shallow mixed-layer in the eastern equatorial and tropical Atlantic favors the persistence of these subsurface anomalies and may explain why the Benguela is particularly sensitive to the biological differential heating. In spite of the presence of high chlorophyll concentrations in the upwelling regions, both the larger amount of shortwave radiation captured in the surface layers and the modifications of the horizontal and vertical advection at the coast are found to play a secondary role in the SST change in the upwelling region.

1. Introduction

The absorption of light by the chlorophyll and related pigments contained in phytoplanktonic biomass modifies the vertical distribution of radiative heating in the upper ocean, with potential implications on the thermal structure and the dynamics of the ocean. The overall importance of this biological effect, also known as self-shading, on the ocean heat budget has been mostly investigated using modeling approaches, either with ocean models [*Nakamoto et al*., 2001; *Murtuggude et al*., 2002; *Manizza et al*., 2005; *Sweeney et al*., 2005; *Park et al*., 2014a,2014b] or with coupled ocean-atmosphere-biogeochemistry models [*Lengaigne et al*., 2007; *Park et al*., 2014a,2014b] which take into account the feedback of biologically driven SST changes on the atmosphere.

In the open ocean and far from the equator, the general agreement is that the dominant response to the biology is 1-D: the absorption of light by the chlorophyll leads to a larger fraction of radiative heating captured by the surface waters while less radiative heating is made available for the subsurface waters. This generally results in a warming of the ocean surface [e.g., *Lengaigne et al*., 2007; *Ma et al*., 2012; *Park et al*., 2014a,2014b] .

In the upwelling regions however, the influence of chlorophyll concentration on SST is still a matter of debate. Most of the studies focused on the Pacific equatorial upwelling region, owing to potential biological feedback on El Niño/La Niña events. Some studies suggest that the differential heating due to chlorophyll leads to a warming of the surface waters of the order of +1°C in the equatorial pacific system [*Timmermann and Jin*, 2002; *Murtuggude et al*., 2002; *Marzeion et al*., 2005; *Wetzel et al*., 2006; *Lengaigne et al*., 2007] while other authors found a sea surface cooling [*Nakamoto et al*., 2001; *Manizza et al*., 2005; *Lin et al*., 2007, 2008, 2011; *Anderson et al*., 2009; *Park et al*., 2014a,2014b]. These results have been summarized in *Park et al*. [2014b]. They are generally sensitive to the type of ocean model used: some authors show that the surface cooling induced by the biology is amplified in fully coupled models relative to forced ocean models

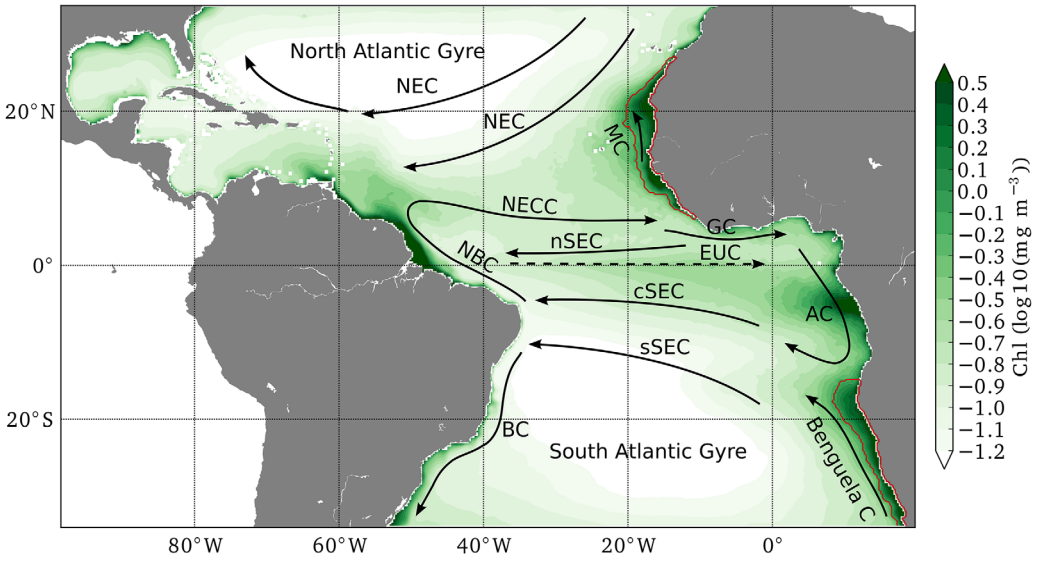

Figure 1. Annual mean of chlorophyll concentrations based on GlobColour monthly merged MODIS/VIIRSN product from 1998 to 2012 with circulation schematic superimposed. The red contours indicate the Senegal and Benguela upwelling regions used for statistics and identified as the regions with annual mean chlorophyll concentrations larger than 1 mg m^{-3}. Surface current branches shown (black solid arrows) are the North Equatorial Current (NEC), the Mauritania Current (MC), the northern, central and south branches of the South Equatorial Current (nSEC, cSEC, and sSEC), the North Equatorial Countercurrent (NECC), the Guinea Current (GC), the Angola Current (AC), the North Brazil Current (NBC), the Brazil Current (BC), and the Benguela Current (Benguela C). The equatorial Undercurrent (EUC) is indicated in black dashed arrows.

[*Park et al*., 2014b], while other studies show an inversion of the anomaly from cool to warm when using an hybrid or a fully coupled model [*Marzeion et al*., 2005; *Lengaigne et al*., 2007]. The diversity of the model responses may arise from the model diversity, which have different bias either in the physics or in the simulated chlorophyll (when using ocean-biogeochemistry coupled models).

Despite a lack of agreement on the sign of the SST response, most of the recent studies generally agree that in the equatorial upwelling regions, the temperature response of the upper layers is affected by both 1-D (local) thermodynamic processes and 2-D advective processes. Different processes that often interact together have been invoked. Most of the studies explain the temperature anomalies (either positive or negative) by modifications of the upwelling that either cancel or amplify the local surface heating due to chlorophyll [*Manizza et al*., 2005; *Marzeoin et al*., 2005; *Nakamoto et al*., 2001; *Loptien et al*., 2009; *Sweeney et al*., 2005; *Lengaigne et al*., 2007; *Lin et al*., 2007, 2008; *Park et al*., 2014b]. What is generally proposed as a modification of the upwelling may involve many different processes (vertical velocity, mixing, vertical gradients of temperature), but we still lack a comprehensive understanding of the dominant processes.

The Tropical Atlantic holds productive upwelling systems (either equatorial or coastal) and marked spatial gradients of chlorophyll concentrations [e.g., *Signorini et al*., 1999] (see also Figure 1), but the impact of the biology in this region has been poorly studied. Using a numerical model, *Frouin et al*. [2007] analyzed the impact of the chlorophyll on the thermal structure and the currents of the Tropical Atlantic Ocean. They observed a warming of 3–4°C in the region of the Guinea Current, and 1–2°C in the region of the North Equatorial Current, the northern part of the South Equatorial Current, and in the Caribbean (the Tropical Atlantic current system is sketched in Figure 1). They observed a cooling of around 1°C in the Benguela upwelling. They show that these modifications coincide with a strengthening of the equatorial currents, but the processes involved in a possible causal relationship between the currents anomalies and the surface temperature anomalies remain to be clarified. Others studies focused on specific areas such as the Guinea Dome [*Duteil et al*., 2009] or the Amazon-Orinoco river plume [*Newinger and Toumi*, 2015], where the impact of the chlorophyll was driven at first order by 1-D processes. So we still lack a comprehensive understanding of the processes at play at the Atlantic basin scale.

The aim of this paper is to evaluate and understand the sensitivity of the Tropical Atlantic upper ocean temperatures to biological differential heating. For that purpose, we analyze a set of interannual (1979–2012)

regional simulations based on a 1/4° model of the Tropical Atlantic, for which different chlorophyll concentrations are specified. The large sensitivity of the Mauritania-Senegal and Benguela upwelling systems led us to primarily focus on these areas. The paper is organized as follows. Section 2 describes the model and the various observational data sets used in the study. Section 3 describes the influence of the biology activity on the Tropical Atlantic. The processes controlling the sea surface response of the coastal upwellings to biological differential heating are analyzed in sections 4 and 5 for the Benguela and Senegal upwelling, respectively. Finally, the results are summarized and discussed in section 6.

2. Data and Methodology

2.1. Regional Model Description

The regional ocean model configuration used in this study is built from the oceanic component of NEMO3.6 (Nucleus for European Modeling of the Ocean) [*Madec*, 2014]. It solves the three dimensional primitive equations discretized on a C-grid and fixed vertical levels (*z*-coordinate) on a regional grid of 1/4° horizontal resolution that encompasses the Tropical Atlantic (35°S–35°N, 100°W–15°E). It has 75 levels in the vertical, with 12 levels in the upper 20 m and 24 levels in the upper 100 m. Such a configuration has already been described in full details in *Hernandez et al*. [2016], a study in which it is shown that the model successfully reproduces the Tropical Atlantic mean state and the sea surface cooling in the wake of tropical storms and hurricanes of the western Tropical Atlantic.

The model is forced at its lateral boundaries with daily outputs from the MERCATOR global reanalysis GLORYS2V3. At the surface, the atmospheric fluxes of momentum, heat, and freshwater are provided by bulk formulae [*Large and Yeager*, 2009]. The model is forced with DFS5.2 product [*Dussin et al*., 2014] which is based on ERAinterim [*Dee et al*., 2011] reanalysis and consists of 3 h fields of wind speed, atmospheric temperature and humidity, and daily fields of longwave, shortwave radiation, and precipitation. DFS5.2 is an update of the product described in *Brodeau et al*. [2010].

A special care was taken in the choice of the shortwave penetration scheme. The parametrization of the solar radiation penetration holds on the principle that light absorption in the ocean is spectrally selective and depends on particle concentration. In all our simulations, the penetration of the solar heat flux radiation Qsr is represented using a three-waveband Red-Green-Blue (RGB) model [*Lengaigne et al*., 2007] based on the full spectral model of *Morel* [1988]. We use the empirical parameterization from *Morel and Berthon* [1989] to calculate a vertical profile of chlorophyll from surface chlorophyll satellite concentration. Figure 2a shows the shortwave penetration profiles obtained for different values of chlorophyll concentrations from 0.05 to 1 mg m^{-3}. The parametrization used for all simulations includes a deep chlorophyll maximum

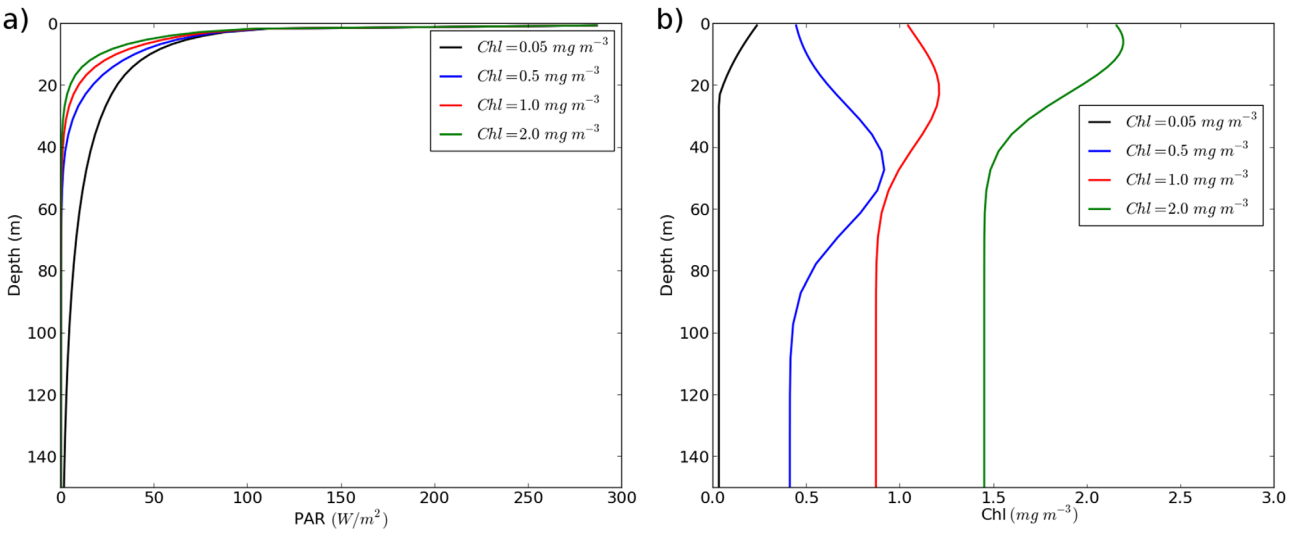

Figure 2. (a) Penetration profile of the photosynthetically available radiation (PAR) calculated with a three-waveband RGB model and a variable profile of chlorophyll concentration shown for different chlorophyll surface concentrations. (b) Corresponding vertical profiles of Chl(z) following the formulation of *Morel and Berthon* [1989].

Table 1. List and Characteristics of the Different Simulations Performed and Analyzed in This Study

Experiment	Chlorophyll Concentration	Integration Period	Initial Conditions
$CHL_{0.05}$	Constant and horizontally homogeneous (0.05 mg m^{-3})	1979–2012	*Levitus* [1998]
CHL_{clim}	Monthly climatology	1979–2012	*Levitus* [1998]
CHL_{cst}	Annual mean climatology	1979–2012	*Levitus* [1998]

(Figure 2b) and is based on the relationship between the near-surface chlorophyll concentration and the column-integrated chlorophyll content. We verified that our results (in terms of SST sensitivity) are not very sensitive to the choice of a varying vertical profile of chlorophyll obtained with the *Morel and Berthon* [1989] parametrization or assuming a vertically homogeneous concentration of chlorophyll as done for example in *Lengaigne et al*. [2007]. Indeed the SST differences between simulations performed with a constant or vertically varying profile of chlorophyll (see Figure Figure A1 in Appendix A) are negligible compared to the sensitivity of the model SST to the total chlorophyll concentration as we will below (e.g., section 3.1).

The simulations that have been performed in this study (Table 1) only differ in the spatial and temporal distribution of the chlorophyll concentrations that are specified. The reference simulation ($CHL_{0.05}$) is forced with a horizontally homogeneous chlorophyll concentration set to 0.05 mg m^{-3}, and different sensitivity experiments are performed: CHL_{clim} is forced with a monthly climatology of chlorophyll concentrations obtained from GlobColour monthly merged product for the period 1998–2012 (details on these data are given in section 2.2). CHL_{cst} is forced with annual mean chlorophyll concentration (i.e., concentration is constant in time).

All experiments were initialized with temperature and salinity climatology provided by the WOA98 Atlas [*Levitus et al*., 1998] on 1 January 1979 and is integrated over the period 1979–2012. The evolution of the temperature anomalies in the upper 200 m shows that the anomalies stabilize after 20 years and that the period 1998–2012 is suitable (see Figure Figure A2). Daily averages from 1998 to 2012 are analyzed to validate the $CHL_{0.05}$ simulation but the comparison between experiments is performed on the period 2005–2012.

2.2. Observations

Time and spatially varying chlorophyll concentrations used to force the model are obtained from satellite data from 1998 to 2012. We use the OSS2015 GlobColour [*Fanton d'Anton et al*., 2009; *Maritorena et al*., 2010] monthly merged MODIS/VIIRSN product (version 4.0) derived from SeaWIFS, MERIS, MODIS, and VIIRS data at 25 km resolution. These fields have been interpolated linearly onto the 1/4° model grid. Seasonal and annual climatologies are calculated using all the data available from 1998 to 2012. Data have been interpolated linearly on the model grid and gaps due to the presence of clouds were filled by bilinear interpolation. The annual mean of chlorophyll concentration in the Tropical Atlantic Ocean is shown in Figure 1. High chlorophyll concentrations are observed in the eastern boundary Benguela and Mauritania-Senegal upwellings, in the equatorial region and in the plume of the large river of the basin (Amazon, Orinoco, Congo). In contrast, the subtropical gyres are chlorophyll depleted with concentrations below 0.05 mg m^{-3}.

The model mean SST distribution is compared to Microwave OI SST observations (http://www.remss.com/measurements/sea-surface-temperature/oisst-description) derived from an optimal interpolation of Tropical Rainfall Measuring Mission (TRMM) Microwave Imager (TMI) data and Advanced Microwave Scanning Radiometer AMSR-E data. Daily data from 1998 to 2012 at 0.25° × 0.25° spatial resolution are used. The model mixed-layer depth (MLD) and barrier layer thickness (BLT) are compared to MLD climatology and BLT climatology of *de Boyer Montégut et al*. [2004, 2007] at 2° × 2° spatial resolution. For both model and observations, the MLD criterion used in this study corresponds to the depth at which density is 0.03 kg m^{-3} larger than the density at 10 m depth. Observations have been interpolated linearly onto the model grid to be compared to model outputs.

Geostrophic currents derived from SSALTO/DUACS altimetry are used to derive the mean satellite eddy kinetic energy (EKE). We use data from 2005 to 2012 for the validation. The EKE is computed from velocity anomalies as $(1/2)(u'^2 + v'^2)$, where u is a model or altimetry-derived geostrophic surface velocity, and u′ the anomaly with respect to the mean seasonal cycle from 2005 to 2012.

2.3. Comparison of the Reference Simulation With the Observations

The annual climatology of observed SST from 1998 to 2012 is shown in Figure 3a. The main features of the observed SST are well reproduced by the model in the reference simulation $CHL_{0.05}$ (Figure 3c), although the model is slightly cooler north and south of the Inter-Tropical Convergence Zone (−0.5°C) and warmer (+1°C) in the Benguela upwelling (Figure 3e). Such warm bias in the Benguela upwelling region is a common feature of low resolution CMIP5 climate models [*Taylor et al*., 2012; *Richter et al*., 2012; *Wang et al*., 2014]. The amplitude of the SST seasonal cycle in the Mauritania-Senegal and Benguela upwelling (defined as the region where the annual mean chlorophyll concentration is higher than 1 mg m^{-3}; see Figure 1) is well reproduced (Figure 3g).

The modeled MLD (Figure 3b) is also in agreement with MLD inferred from observations (Figure 3d) [*de Boyer Montégut et al*., 2004]. Although simulated MLD is around 5 m thicker (Figure 3f), simulated and observed MLD present the same large scale pattern. Monthly differences are particularly important in the Benguela region in August and September (Figure 3g). The poor data coverage (hashed contours in (Figure 3a) in this nearshore area in the observed product may contribute to this difference. We note that the mean MLD (Figures 3b and 3d) is shallow in the equatorial band and in the eastern part of the Tropical Atlantic basin (O ∼ 20 m), and it deepens to 60 m in the subtropical gyres. In the Benguela upwelling, the maximum of MLD is in phase with the austral winter minimum of SST.

2.4. Methods

2.4.1. Heat Budget

To identify the processes responsible for temperature anomalies, the different contributions to heat budget have been computed online. The full three-dimensional temperature equation of the ocean model reads:

$$\partial_t T = \underbrace{\left(u\partial_x T + v\partial_y T + w\partial_z T\right)}_{\text{t\_adv}} + \underbrace{D_l(T)}_{\text{t\_ldf}} + \underbrace{\frac{\partial}{\partial_z}\left(K_z \frac{\partial_T}{\partial_z}\right)}_{\text{t\_zdf}} + \underbrace{\frac{Q_{ns}}{\rho_0 C_p \Delta z} + I(z)}_{\text{t\_flx}} \quad (1)$$

where T is the model potential temperature, (u, v, w) are the components of the ocean currents, $D_l(T)$ is the lateral diffusion operator, K_z is the vertical diffusion coefficient, C_p is the specific heat of sea water, ρ_0 is the reference density, Δz is the thickness of the first grid cell, and $I(z) = Q_s\, \partial_z f(z)$ is the heating rate due to the penetrative solar heat flux with Q_s the net surface solar heat flux and $f(z)$ the fraction of the solar radiation that reaches depth z. The term t_adv represents the advection of temperature, t_ldf and t_zdf are the lateral and vertical diffusion of temperature, respectively, and t_flx is the air-sea heat flux, including both the penetrative shortwave radiation contribution and the nonsolar contributions. The differences between the sensitivity experiments will be caused by different vertical profiles of $I(z)$, due to different absorption of the penetrative solar radiation.

3. Influence of the Biological Activity on the Tropical Atlantic

3.1. Mean State

Temperature differences in the ML between the simulations CHL_{clim} (climatological chlorophyll forcing) and $CHL_{0.05}$ (clear waters; reference simulation) show a warming in the open ocean everywhere CHL_{clim} chlorophyll concentrations are lower compared to $CHL_{0.05}$ chlorophyll concentrations. The largest warming (∼0.3°C) is observed near the plume areas, especially in the Congo river plume near 6°S. In contrast, the main upwelling systems, which are regions with high chlorophyll concentration, cool down (Figure 4a). This cooling reaches ∼1°C in the Benguela, Mauritania-Senegal, and southern Caribbean upwelling systems. A cooling is also observed in the equatorial upwelling, but it is weaker (∼0.5°C). The net air-sea heat flux anomalies (Figure 4b) tend to compensate the temperature anomalies: they warm (+20 W m^{-2}) the upwelling regions, and thus weaken the SST anomalies.

The MLD is significantly impacted by the biology. It is 10–20 m shallower in and offshore the Mauritania-Senegal and Benguela upwellings where the MLD is already shallow (10–30 m deep, Figure 3d). Below the mixed-layer, there is a basin scale cooling in CHL_{clim} almost everywhere where chlorophyll concentrations are larger than the constant value used in the simulation $CHL_{0.05}$ (Figure 4c). Surface currents are slightly increased at the western boundary in CHL_{clim} (∼5 cm s^{-1}), but changes are relatively weak at the eastern boundary (Figure 4e).

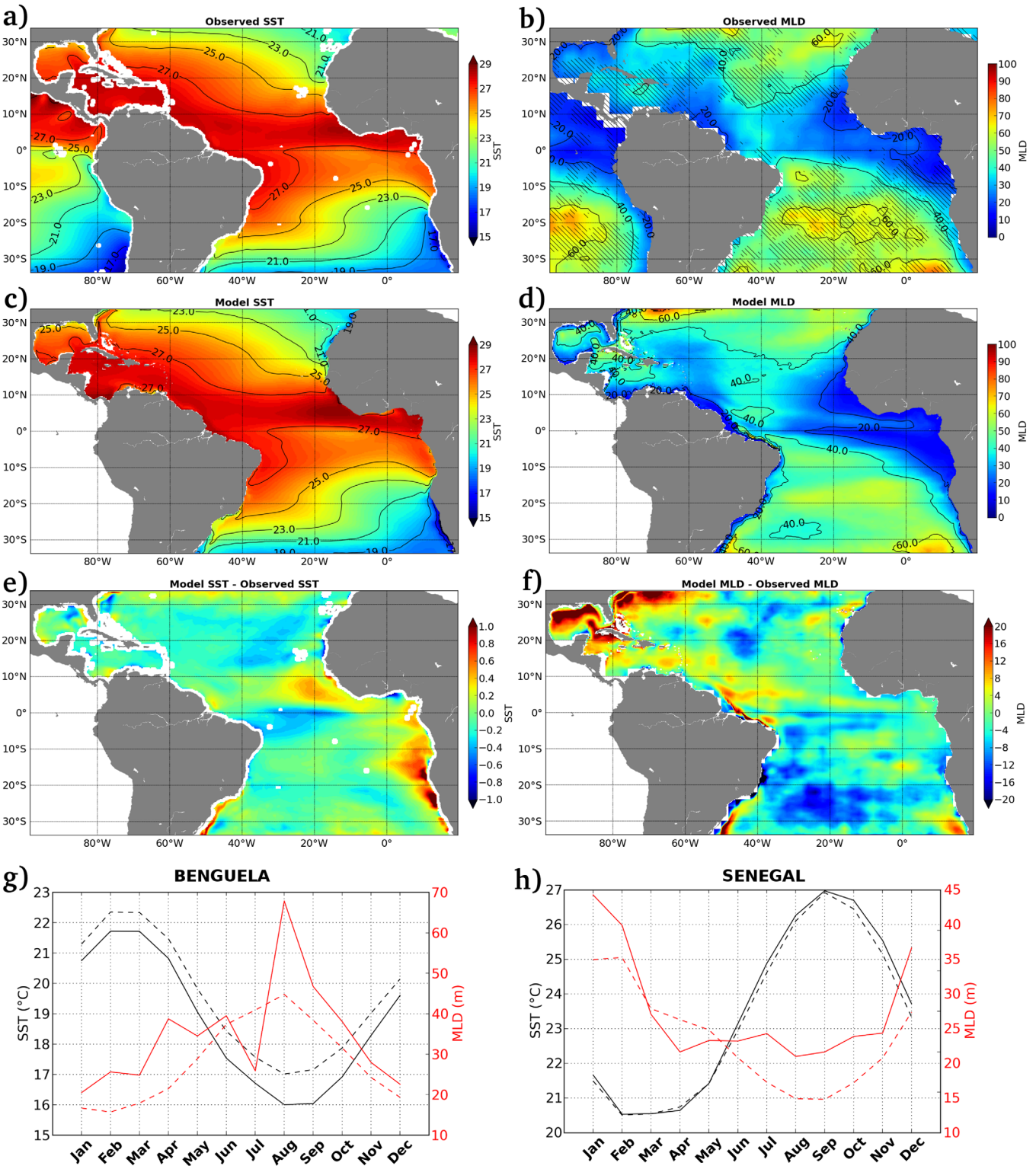

Figure 3. Annual climatological SST (°C; left) and MLD (meters; right) from (a and b) observations and (c and d) model. The differences between model and observations are shown in Figures 3e and 3f. Observed SST are from OI microwave data set and observed MLD data are from *de Boyer Montegut* [2004]. (g and h) Mean seasonal cycle of SST (black) and MLD (red) for the Benguela and Senegal region (as defined in Figure 1) for the model (dotted line) and observations (continuous line). In b) hashed contours indicate grid point (of 2° × 2°) where less than five profiles have been use to build the climatology.

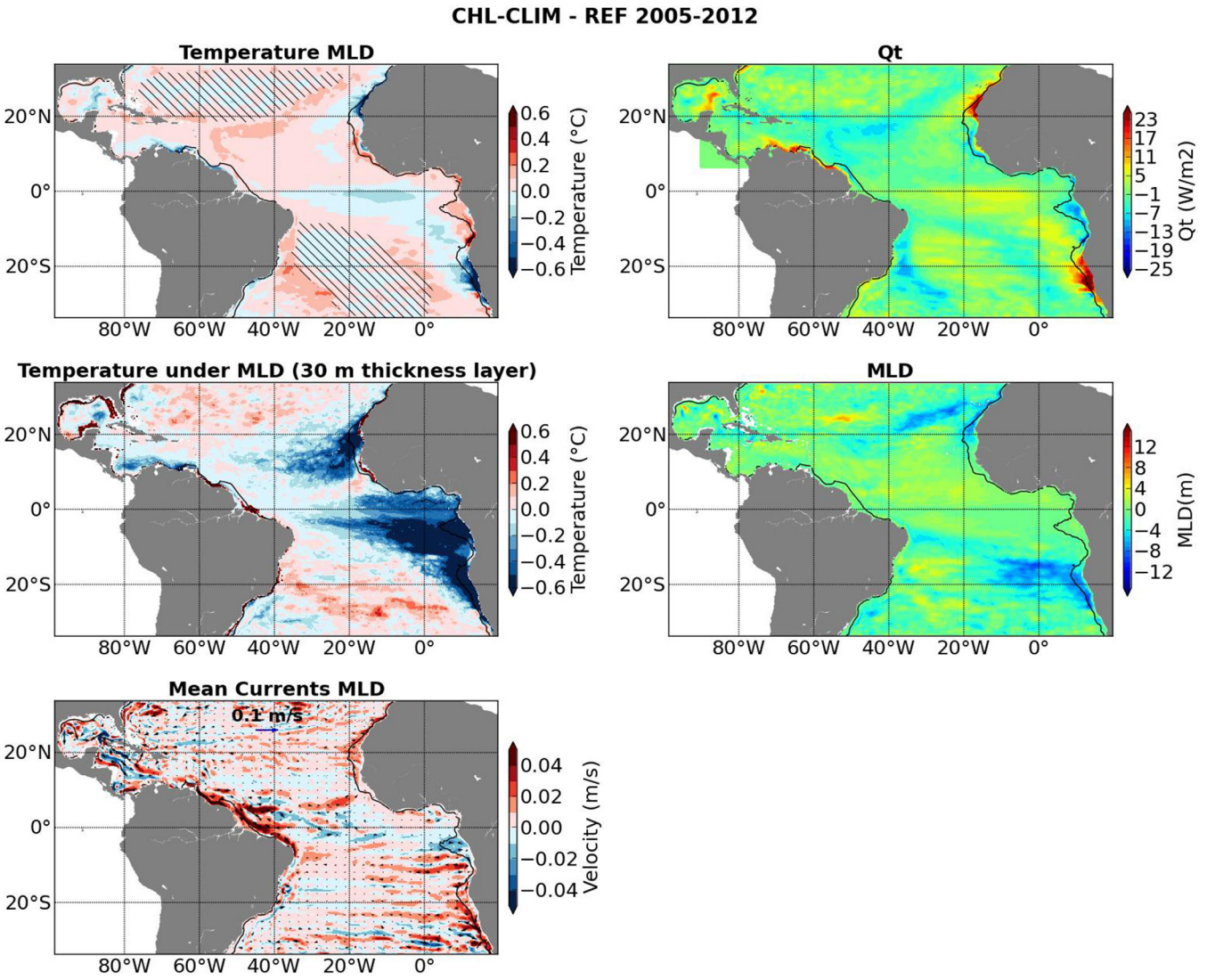

Figure 4. Differences between the simulation with climatological chlorophyll (CHL_{CLIM}) and the model reference simulation ($CHL_{0.05}$) averaged from 2005 to 2012. (a) Mixed-layer temperature anomalies (°C), (b) net air-sea heat flux Qt anomalies (W m^{-2}), (c) anomalies of temperature averaged in a 30 m thick layer under the mixed-layer depth, (d) MLD anomalies (m), and (e) surface currents anomalies (m s^{-1}). Black line indicates the 1 mg m^{-3} annual mean chlorophyll concentration contour. Hashed contours indicate the region where chlorophyll concentration in CHL_{CLIM} simulation is lower than 0.05 mg m^{-3} at least during one month within a season.

3.2. Seasonality of the Temperature Anomaly

The analysis of the seasonality of the temperature anomalies in the ML (Figure 5) shows permanent cooling anomalies in the Benguela region between 27°S and 20°S and in the north of the Mauritania-Senegal region from 20°N to 26°N as already observed in Figure 4a. In the remainder of the paper, we will mainly focus on these areas where permanent cooling anomalies are observed, which coincide with regions of permanent upwelling. However, it is worth mentioning that the temperature anomalies have marked seasonality in terms of amplitude and horizontal extent: in the Mauritania-Senegal region, the temperature anomalies seasonally extend to the south from 20°N to 12°N between February and April. In the Benguela region, cold anomalies are higher between May and June. These seasonal variations of the anomalies are closely related to the seasonality of these upwellings [see *Cury and Shannon*, 2004; *Cropper et al*., 2014; *Fischer et al*., 2016].

In the equatorial region, the temperature anomalies between CHL_{clim} and CHL_{005} are negative almost throughout the year but show a marked peak from May to August. In the Congo river plume (located around 5°S and identified by the 1 mg m^{-3} isocontour in Figure 5), temperature anomalies follow a nontrivial seasonal cycle. During a large part of the year, the river plume is warmer in CHL_{clim}. This warming is

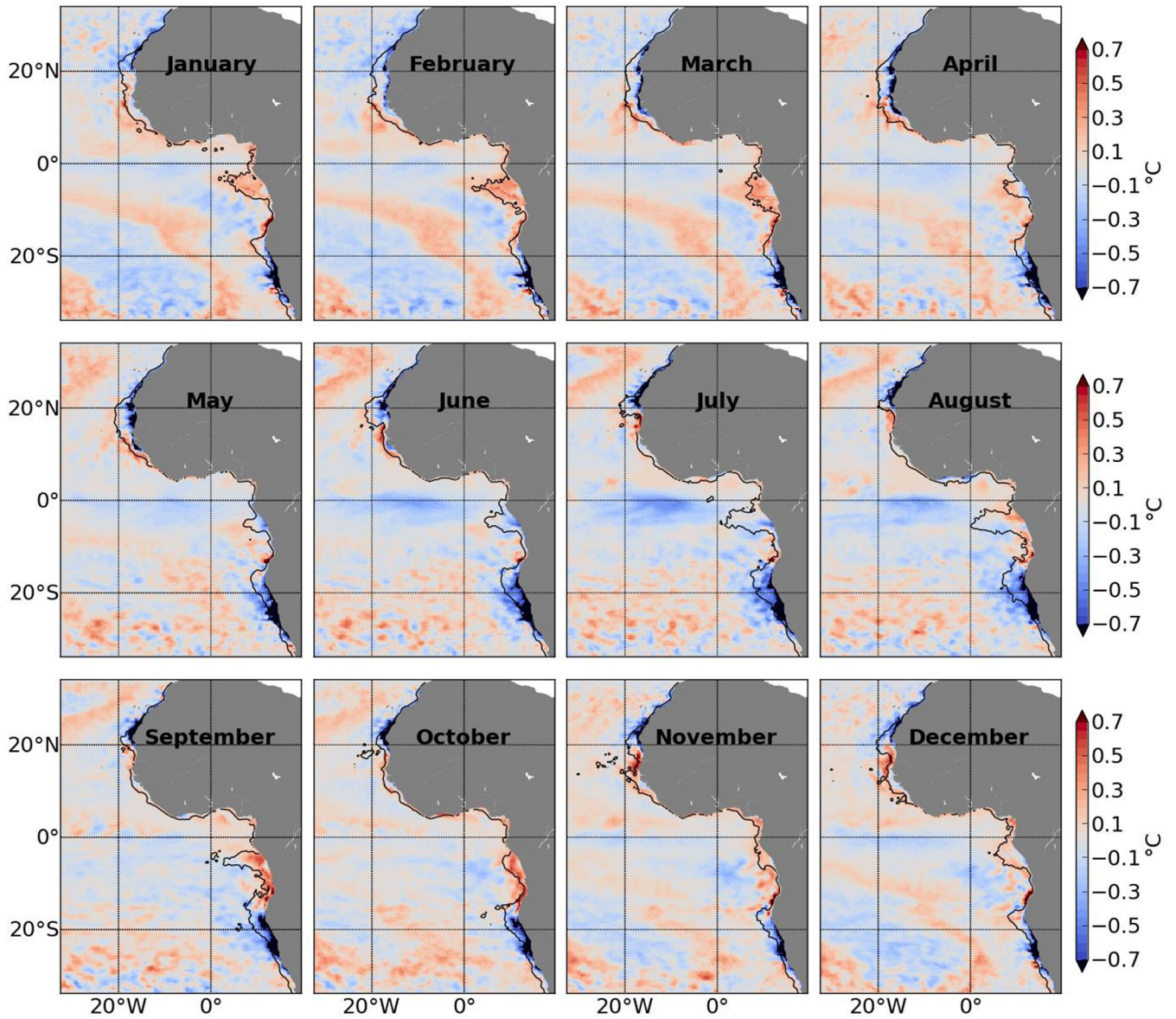

Figure 5. Differences of monthly temperature in the mixed-layer (in °C) between the simulation with climatological chlorophyll (CHL_{CLIM}) and the model reference simulation ($CHL_{0.05}$), averaged from 2005 to 2012. Black lines indicate the 1 mg m^{-3} monthly mean chlorophyll concentration iso-contour.

expected and is explained by the 1-D process already mentioned in the introduction section: in presence of chlorophyll more heat is captured in the surface layer. But interestingly, surface temperatures in May–June–July are lower in CHL_{clim}. These two peaks of negative temperature anomalies (at the equator and in the river plume) occur during the peak season of the Atlantic cold tongue [e.g., *Jouanno et al.*, 2011a], which extends from 35°W at the equator to the African coast, where it can reach the Congo plume area [e.g., *Jouanno et al.*, 2011b]. During this season, an important amount of subsurface waters is brought to the surface by upwelling and mixing in response to the seasonal variability of the equatorial winds. So we expect the anomalously cool subsurface waters (Figure 4c) to upwell during this season and to compensate the surface warming.

3.3. Impact of the Seasonal Variability of Chl

In the Benguela upwelling, the maximum of SST negative anomalies occurs in April concomitantly with the presence of a maximum in chlorophyll at this period (Figures 5 and 6a, 6b). This indicates that the

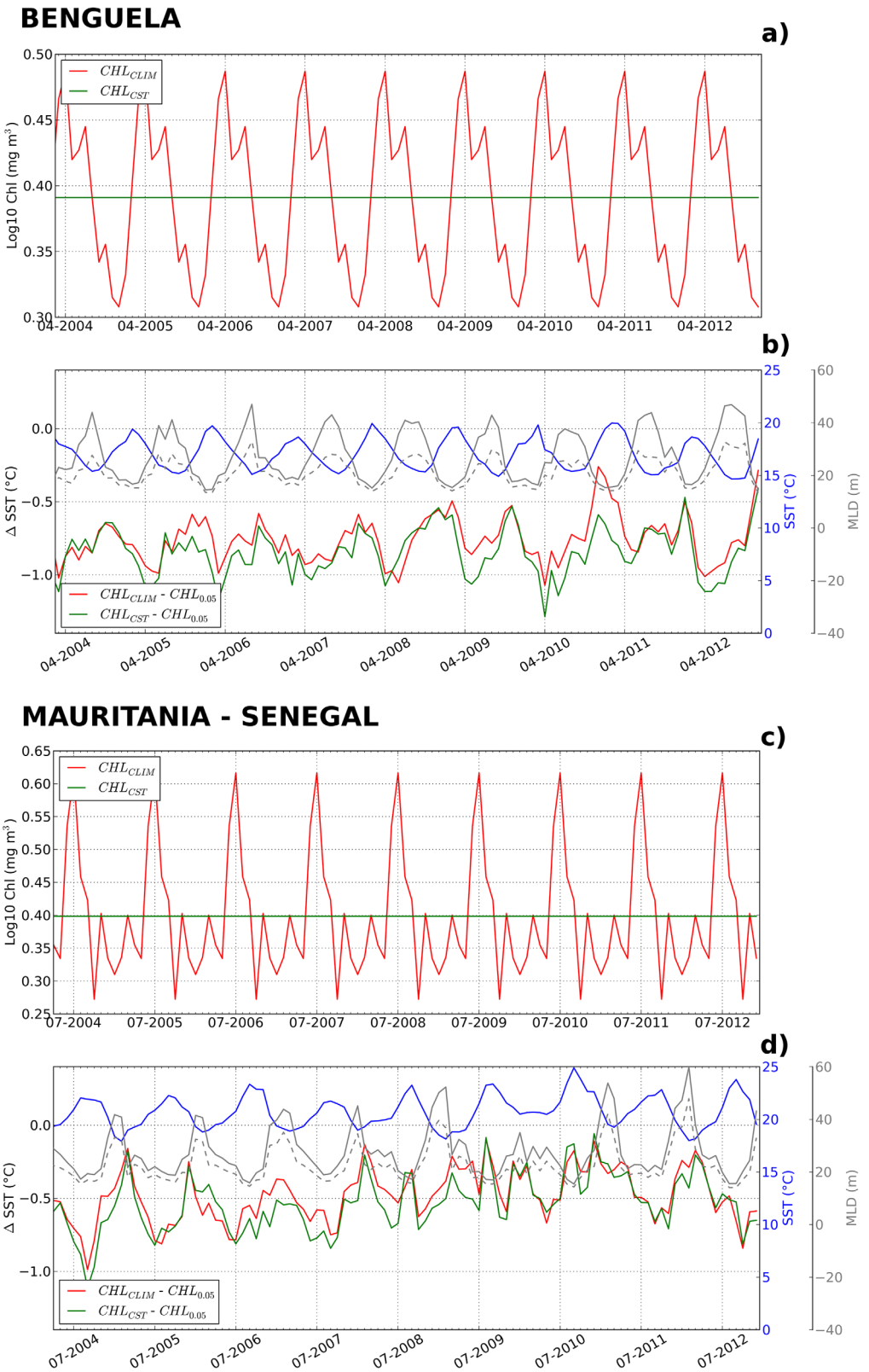

Figure 6. (a) Chlorophyll concentrations in CHL_{clim} and CHL_{cst} (mg m^{-3}), (b) anomalies (compared to $CHL_{0.05}$) of sea surface temperature average in the Benguela upwelling region between 27°S and 20°S for CHL_{clim} (red) and CHL_{cst} (green). Gray dotted line corresponds to CHL_{clim} mixed-layer depth and gray continuous line to $CHL_{0.05}$ mixed-layer depth. The blue line represents the SST for simulation $CHL_{0.05}$. (c and d) The same but for the Mauritania-Senegal upwelling region averaged between 20°N and 26°N.

seasonality of the anomaly is not driven by the local variability of the chlorophyll concentrations (if there were be a link between both, we would expect a decrease of the surface temperature anomalies when chlorophyll concentrations are at their highest). Furthermore, the temperature anomalies (with respect to $CHL_{0.05}$) obtained in the simulation forced with annual mean chlorophyll concentration (CHL_{cst}) are very close to CHL_{clim} (Figure 6b). This suggests that the seasonal cycle in chlorophyll concentrations, neither locally nor at the basin scale, is not the first-order mechanism driving the seasonal cycle of the anomalies. In the Mauritania-Senegal upwelling, there are no major differences between CHL_{clim} and CHL_{cst} in spite of a large chlorophyll variability (Figures 6c and 6d) suggesting also that seasonal variability of the temperature anomalies are not driven by the variability of the chlorophyll concentration.

4. Mechanisms in the Benguela Upwelling

As already described in previous studies, the processes responsible for the surface warming and subsurface cooling outside the upwelling regions are one-dimensional and relatively well understood: more heat is captured in the top layers by the chlorophyll while less heat is available at the subsurface. This is illustrated in Figure 7a which displays the difference in radiative heating rates between CHL_{clim} and $CHL_{0.05}$ along a zonal section crossing the Benguela upwelling system (meridionally averaged between 27°S and 20°S). We see that close to the coast the heating difference between the surface and the subsurface is increased. We also note that near the coast, the heating anomaly in the 0–10 m surface layer is positive despite the observed surface cooling in CHL_{clim}. Thus, the cold anomaly observed in the upwelling region in CHL_{clim} cannot be explained by a local modulation of the shortwave heat flux. Other processes are involved and they are investigated in the following sections.

4.1. Lagrangian Analysis

One hypothesis to explain the cooling in upwelling regions is that the temperature anomalies could be formed upstream, offshore of the upwelling area. To test this hypothesis, we performed a Lagrangian analysis using ARIANE for the $CHL_{0.05}$ and CHL_{clim} experiments. The origin of the water masses that upwell in the Benguela upwelling is explored by tracking 4 years backward in time the waters masses that upwell. To do that, we use the offline Lagrangian tool ARIANE [*Blanke and Raynaud*, 1997; *Blanke et al*., 1999]. Lagrangian analysis was performed using daily average outputs of $CHL_{0.05}$ and CHL_{clim} experiments. A total amount of 135,687 particles were released each day from 1 January 2008 to 31 December 2012 from 20°S to 27°S. At 25 km resolution, the Benguela upwelling is very coastal (Figure 7b) and thus we decided to release the particles at the first ocean grid point at the coast, at 20, 40, and 60 m depth. The particles were integrated backward during 4 years and the temperature, the age, and the depth of each particle were recorded along each trajectory every 5 days. The different contributions to the temperature evolution were also recorded along the particle trajectories in order to identify the processes responsible for the temperature anomalies within the upwelling.

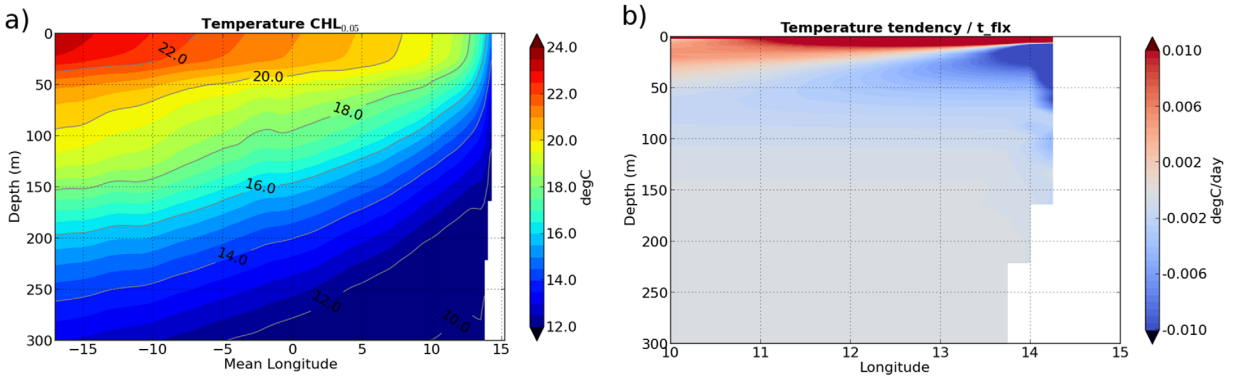

Figure 7. Mean zonal section in the Benguela region (between 27°S and 20°S) for (a) difference of surface forcing heating rate (°C/d, term t_flx see equation (1)) between CHL_{clim} and $CHL_{0.05}$. (b) Mean temperature in $CHL_{0.05}$ simulation. Data from 2005 to 2012 are used.

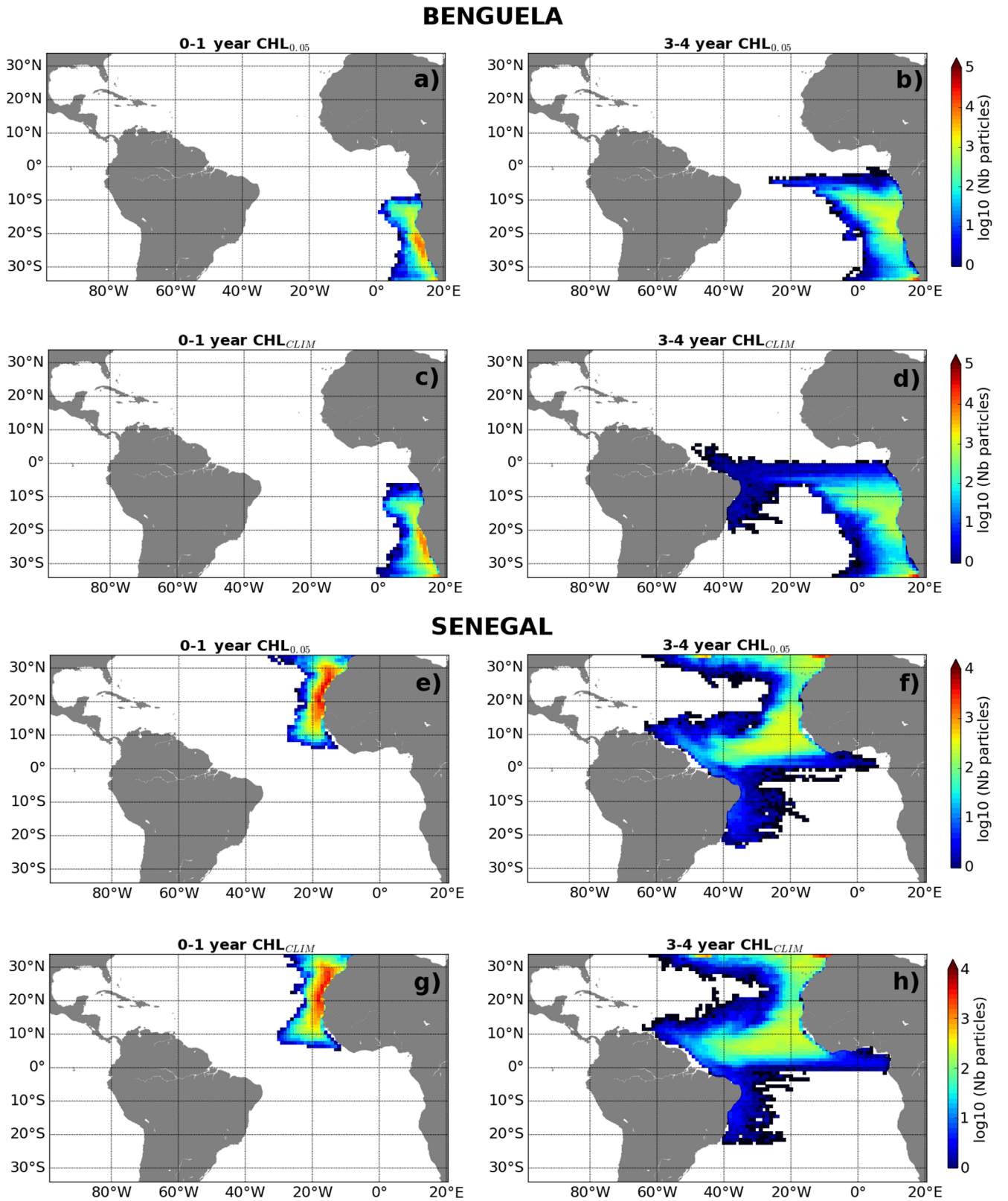

Figure 8. Repartition for the first and fourth year of backward integration of particles seeded in the (a–d) Benguela and (e–h) Mauritania-Senegal upwelling systems. The particles were released daily from 2008 to 2012 at 20, 40, and 60 m depth at each grid cell closest to the coast from 20°S and 27°S for the Benguela upwelling and from 20°N and 26°N for the Mauritania-Senegal upwelling.

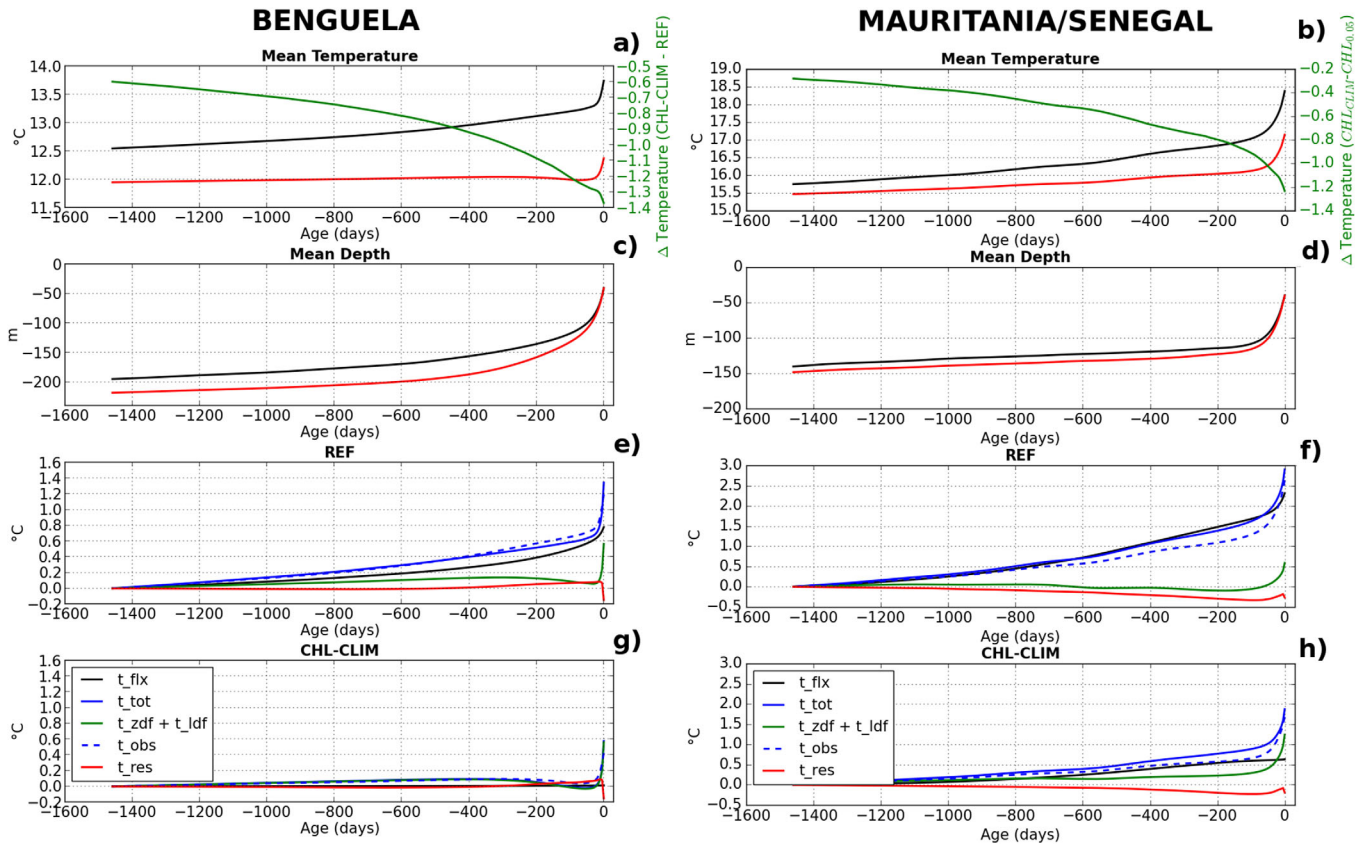

Figure 9. Averaged properties as a function of their age for all the particles seeded in the Benguela upwelling (left) and in the Senegal-Mauritania upwelling during the period 2005–2012: (a and b) temperature, (c and d) depth. The temperature t_tot (°C), in plots (e and f) for CHL0.05 and (g and h) for CHLclim (g and h), is the sum of the temperatures obtained as the integration (from year −4 to the seeding time) of the surface forcing trends (t_flx) and the diffusive trends (t_zdf + t_ldf). The difference (i.e., the residual) between t_tot and the evolution of the temperature averaged for all the water parcels (t_obs) is shown as t_res.

In a Lagrangian framework the heat budget of a water parcel reduces to:

$$\partial_t T = \underbrace{D_l(T)}_{\text{t\_ldf}} + \underbrace{\frac{\partial}{\partial_z}\left(K_z \frac{\partial_T}{\partial_z}\right)}_{\text{t\_zdf}} + \underbrace{\frac{Q_{ns}}{\rho_0 C_p \Delta z} + I(z)}_{\text{t\_flx}} \quad (2)$$

The temperature, position, depth, and heat balance averaged over all the particles are analyzed as a function of their age (Figures 8 and 9). Figure 8 shows the distribution of the particles during the first and fourth year of backward integration. The analysis shows that during the first year prior to their arrival at the coast the particles were located relatively close to the upwelling regions. The distribution of the particles the years before indicates that a large fraction of the waters is advected from the equatorial or near equatorial regions and another fraction is advected from the south (Figure 8). During the first year, 12% of the trajectories in $CHL_{0.05}$ and 27% of the trajectories in CHL_{clim} have been intercepted at 33°S (Table 2). During the fourth year, these values raised to 29% and 48%, respectively. This indicates significant changes in the advection pathways between the two simulations. Note that for the diagnostics discussed in the next section, we will retain all the pathways, keeping the properties of the water parcels (temperature, depth) constant south of 33°S previous to their entrance within the domain.

Table 2. Numbers of Trajectories That Have Been Intercepted at 33°S During the First, Second, Third, and Fourth Years Prior to Their Arrival to the Benguela Upwelling

	Ntraj $CHL_{0.05}$	Ntraj CHL_{clim}
First year	12%	27%
Second year	23%	43%
Third year	27%	47%
Fourth year	29%	48%

At seeding time (age = 0 days; Figure 9a), the temperature difference between $CHL_{0.05}$ and CHL_{clim} is ~1.37°C. A temperature anomaly of 0.60°C (43.8% of the total anomaly) is already present at the backward integration

Table 3. Contribution of the Heat Budget Terms (Total Tendency, Mixing, and Surface Flux) to the 4 Year Average Temperature Tendency Following all the Trajectories[a]

		Total Number of Particles	Total Temperature Tendency (°C, t_tot)	Total Mixing (°C, t_ldf + t_zdf)	Surface Heat Flux (°C, t_flx))
$CHL_{0.05}$	Total	39,756,291	1.35	0.57	0.78
	[chl] <= 1 mg m^{-3}	25,338,018	0.42	0.14	0.28
	[chl] > 1 mg m^{-3}	14,418,273	0.92	0.42	0.50
$CHL_{0.05}$ with advection CHL_{clim}	39,756,291	1.30	0.54	0.75	
CHL_{clim}	Total	39,756,291	0.58	0.56	0.015
	[chl] <= 1 mg m^{-3}	25,789,126	0.13	0.13	0.007
	[chl] > 1 mg m^{-3}	13,967,165	0.45	0.44	0.008
CHL_{clim} with advection $CHL_{0.05}$	39,756,291	0.53	0.52	0.012	

[a]The term are computed in the entire model domain and in regions with surface chlorophyll larger and weaker than 1 mg m^{-3}. This distinction aims at roughly distinguishing particles located in and out the upwelling areas.

time limit (i.e., fourth-year backward). We cannot fully conclude on the origin of this anomaly, but the difference in the origin depth (~30 m deeper when taking into account realistic chlorophyll concentrations; Figures 9c and 9d) suggests it is due to changes in the advection pathways. The remaining 0.77°C (56.2%) of the temperature anomaly is explained by a reduction of subsurface heating (t_flx) when considering realistic chlorophyll concentrations. Indeed, in $CHL_{0.05}$ the particles get warmed throughout their trajectories while this warming is much weaker (almost nonexistent) in CHL_{clim} (Figure 9a).

Although the temperature anomaly is forming long before waters enter the upwelling system (green curve in Figure 9a), around ~0.43°C (31.4%) of the temperature anomaly is formed during the last year before the waters reach the upwelling cell, due to the fact that water parcels enter a region of enhanced surface chlorophyll (Figures 2 and 8a). The effect is accelerated during the last year previous to upwelling because (i) the particles get closer to the upwelling region so the shading effect is larger due to larger chlorophyll concentrations and (ii) the particles get shallower so the differences of penetrative solar radiation are larger.

A heat budget following the particles has been performed to shed light on the processes contributing to the different temperature evolutions along the particle paths in CHL_{clim} and $CHL_{0.05}$. The temperature tendency of each water parcel (t_tot in °C/month) can be decomposed as the sum of a diffusive contribution (t_ldf+t_zdf) and air-sea fluxes contribution (t_flx) (see equation (2)). These contributions were calculated online for each grid point, and then interpolated along the particles backward trajectories using ARIANE, and integrated forward in time along the trajectories from year −4 (Figures 9e and 9f). We can verify that the difference between the total temperature tendency and the sum of the diffusive and air-sea fluxes contribution is small and lower than 0.2°C (see the residual term t_res shown in Figure 9 which is the difference between the temperature tendency seen by a water parcel and the sum of the diffusive and air-sea fluxes contributions). This residual comes from numerical errors due to interpolation along the trajectories. The 1.37°C average warming of the water parcels in $CHL_{0.05}$ is explained by both mixing (+0.57°C) and air-sea fluxes (+0.78°C; see Table 3). The analysis of the different terms of the heat budget following the water parcels reveals that radiative heating (t_flx) is the main process that warms the water parcels in $CHL_{0.05}$ along their way to the upwelling, while horizontal and vertical diffusions have an impact only during the few days before the waters reach the upwelling cell. The significant contribution of the diffusion at this stage is explained by the intense vertical mixing that occurs within the upwellings [e.g., *Renault et al*., 2011; *Jouanno and Sheinbaum*, 2013]. In contrast, the air-sea fluxes have almost no impact on the local temperature tendency of the particles in CHL_{clim} (Figure 9g). Indeed, the air-sea fluxes only contribute to 0.015°C of the 0.58°C warming, while 0.56°C is due to the mixing contribution (Table 3). The straightforward interpretation for such difference between CHL_{clim} and $CHL_{0.05}$ is that the chlorophyll concentrations limit the shortwave radiations that reach the subsurface.

To further disentangle the role of the high chlorophyll concentrations in the upwelling area versus the role of the weaker chlorophyll concentrations found in open ocean waters, we computed the fraction of radiative warming of the water parcels as a function of chlorophyll concentrations. A large amount of the shading effect is achieved in regions with relatively low surface chlorophyll concentration (Figures 10c and 10d). We found that 64% of the final temperature anomaly between the two

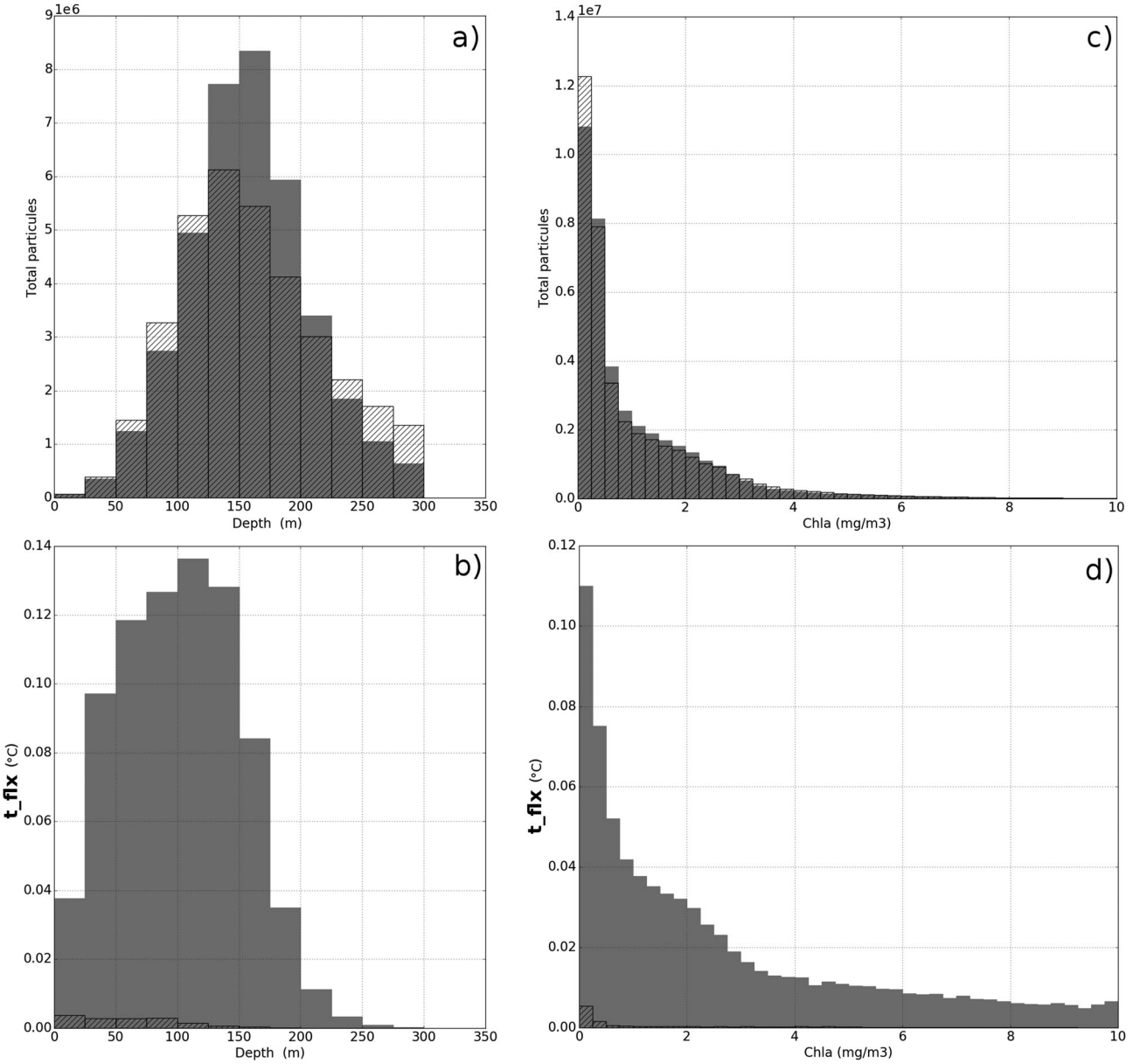

Figure 10. (a) Depth distribution of the particles (we considered all the particles and the full Lagrangian backward integration period, i.e., 4 years). (b) Depth distribution of the 4 year mean radiative warming experienced by the water parcels (in °C). (c) Distribution of the water parcels as a function of the surface chlorophyll concentration. (d) Distribution of the 4 year mean radiative warming as a function of the surface chlorophyll concentrations (in °C). Gray bars correspond to $CHL_{0.05}$ simulation and black hashed bars correspond to CHL_{clim} simulation. In both (b) and (d), the sum of the contributions equals to 0.78°C (for $CHL_{0.05}$) and 0.015°C (for CHL_{clim}), and corresponds to the average radiative warming experienced by the water parcels during the 4 years period.

simulations is generated in regions with surface chlorophyll concentration higher than 1 mg m^{-3} while the remaining 36% of the anomaly is created in regions with surface chlorophyll concentration lower than 1 mg m^{-3} (see Table 3). This indicates that near-oligotrophic regions significantly contribute to the temperature anomalies.

Moreover, we notice in Figures 9a and 9b that a large fraction of the difference between the two simulations forms at an average depth of 150–200 m. This is somewhat surprising since the insolation felt at these depths is very weak even in very clear waters (~0.5% of the surface radiation reach 150 m depth for $CHL_{0.05}$ simulation). The fraction of radiative warming computed as a function of the depth indicates that although the mean depth of the particles is between 150 and 200 m, most of the difference of radiative warming is felt by the shallower particles located at depth between 50 and 150 m (Figures 10a and 10b).

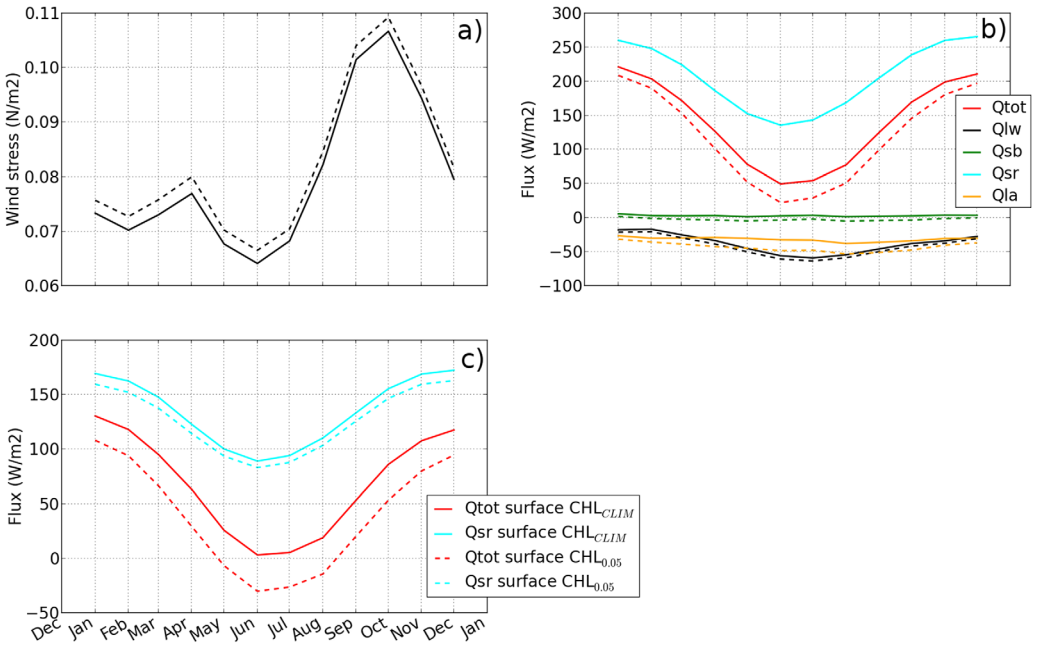

Figure 11. Seasonal evolution for $CHL_{0.05}$ (continuous lines) and CHL_{clim} (dashed lines) in the Benguela upwelling region of (a) the wind stress and (b) the different contributions to the net air-sea heat flux (W m^{-2}): Qtot (total), Qlw (longwave), Qsb (sensible), Qla (latent), *and* Qsr (shortwave radiation). In Figure 11c, Qtot and Qsr are shown the first model cell only.

In order to determine whether differences in the water pathways could explain the temperature differences in the upwelling region, we integrated the heat budget using temperature tendencies of $CHL_{0.05}$ on the trajectories obtained from CHL_{clim}, and conversely (Table 3). The total temperature tendency, together with the corresponding diffusive and air-sea contributions, are found to be very similar to the tendency observed when integrating consistently the tendencies on the trajectories obtained from the same simulation. This suggests that the modification of the water pathways is not the leading mechanism that explains the differences of SST between $CHL_{0.05}$ and CHL_{clim}.

4.2. Seasonal Cycle of the Anomalies

The anomalies of surface temperature due to the effect of chlorophyll concentration follow a seasonal cycle as indicated in section 3.1. In the Benguela upwelling, surface temperatures are minimum at the end of the austral winter and at the beginning of the austral autumn, between July and November (Figures (5 and 7), and 12a). During this period the mixed-layer depth reaches its maximum (Figure 12a). Negative surface temperatures anomalies between CHL_{clim} and $CHL_{0.05}$ are strongest in April–June, when the mixed-layer deepens (Figure 12b). As discussed in section 3.3, this seasonality of the surface temperature anomaly cannot be explained by the local or remote seasonal cycle of the chlorophyll concentrations.

In order to explain such seasonal evolution of the anomaly, we now analyze the heat budget terms for $CHL_{0.05}$ averaged over the Benguela upwelling area and the differences with the trends in CHL_{clim} (Figures 11c and 11h). The total temperature tendency (Figure 12c) has been decomposed into (i) a forcing contribution (sum of solar and non solar air-sea fluxes; Figure 12e) which acts to warm the upper ocean all year long and (ii) a dynamical contribution (sum of advection and diffusion; Figure 12g) which cool the mixed-layer throughout the year.

From October to February (austral summer), the stronger solar heat flux penetrates deeper (Figure 12e) leading to larger deficit of the subsurface radiative heating in CHL_{clim} during this period (Figure 12f). From December to April, the warm surface temperature and shallow mixed-layer, associated with reduced mixing (Figure 12g) strengthen the cool subsurface temperature anomaly (Figure 12b). At the beginning of austral spring (April), the upwelling intensifies as suggested by the shoaling of the isopycnals (Figure 12a) and the strengthening of the contribution of the dynamical processes (vertical diffusion and advection) to the cooling in the upper ocean (Figure 12g). It is during this period that the surface temperature anomaly between

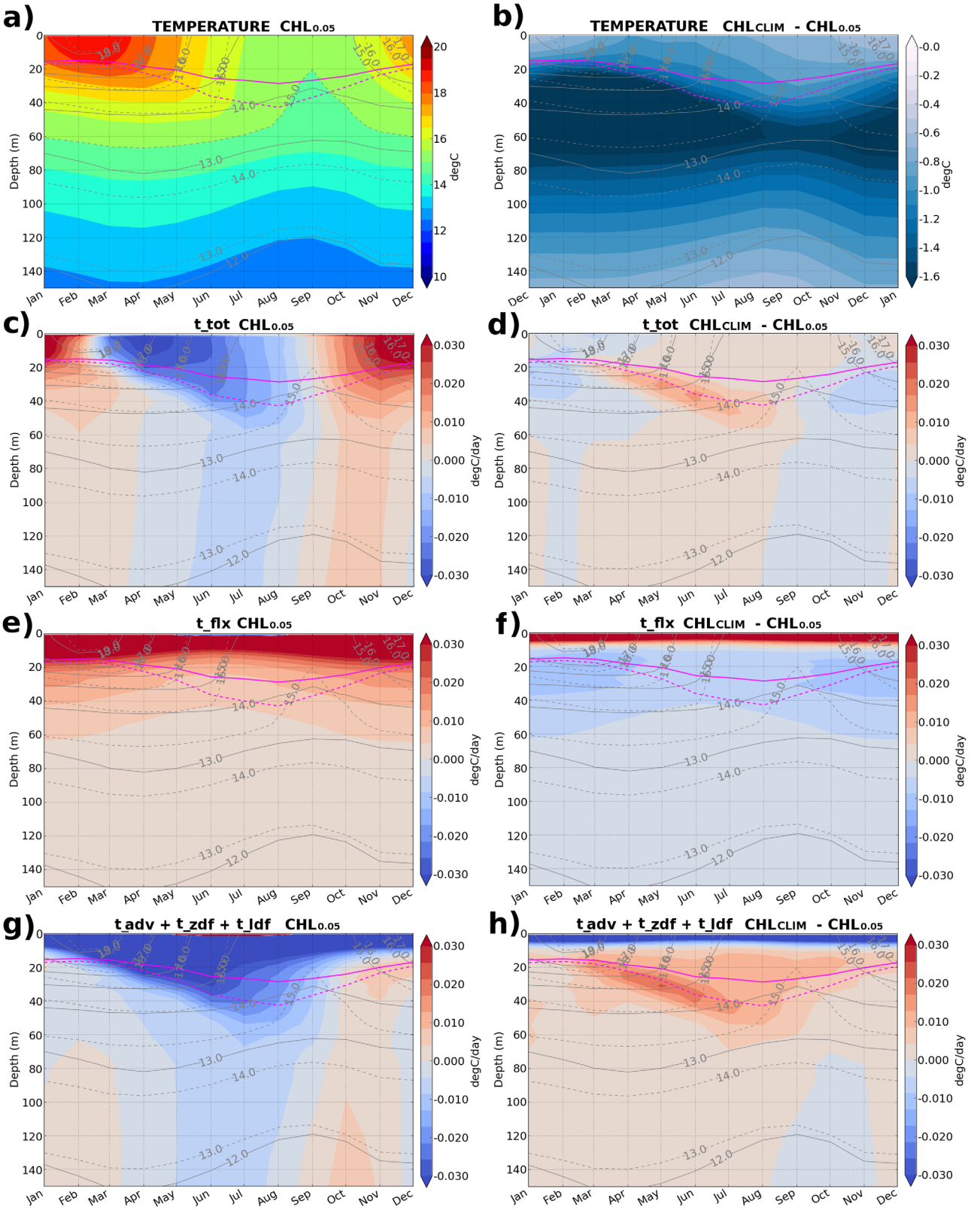

Figure 12. Time-depth evolution of temperature (°C) and the different contributions to model temperature equation (°C d^{-1}; see equation (1)) in the Benguela upwelling region (as defined in Figure 1 and between 27°S and 20°S) for $CHL_{0.05}$ simulation (left) and the difference between CHL_{clim} and $CHL_{0.05}$ (right): (a and b) temperature, (c and d) t tot the total tendency, (e and f) t_flx the air-sea fluxes contribution, and (g and h) the sum of all dynamical contributions to the heat budget (t_adv,t_zdf,t_ldf). Contours of temperature with 1°C interval are superimposed on all the figures, together with the mixed-layer depth (magenta lines), with dotted lines corresponding to $CHL_{0.05}$ and continuous lines to CHL_{clim} isotherm.

CHL_{clim} and $CHL_{0.05}$ is larger (Figure 12b), most probably fed by the bulge of negative anomalies available at subsurface, in response to the deepening of the mixed-layer that occurs in April–June (Figure 12a) bringing anomalously cold waters at the surface.

Interestingly, the seasonal deepening of the mixed-layer seems to be largely influenced by the air-sea fluxes and convective processes rather than by dynamical processes: (1) the wind stress is not particularly strong during this period (Figure 11a), (2) the period of deepening of the mixed-layer corresponds to the period with negative net air-sea flux in the model surface cell (Figure 11b, so it will trigger convective instability), (3) the deepening of the ML is strongly limited in CHL_{clim} in agreement with net air-sea fluxes in the upper cell of the model that remain positive (Figure 11b). Note that these differences in the air-sea fluxes are explained at first order by a weakening of the latent heat fluxes in CHL_{clim} owing to lower SSTs (Figure 11b).

5. Mauritania-Senegal Upwelling

The processes involved in the sensitivity of the Mauritania-Senegal upwelling to biology are very similar to those described for the Benguela upwelling in the previous section. The Lagrangian analysis (109,424 particles released in the Mauritania-Senegal upwelling from 20°N to 26°N each day from 1 January 2008 to 31 December 2012) indicates that a large fraction of the waters that upwell in the Mauritania-Senegal upwelling is advected from the north: 4 years before the seeding time, 47% and 49% of the water parcels crossed the northern boundary, while the other fraction is mainly advected from the equatorial or near equatorial regions (Figures 8f and 8h). As in the Benguela, a large fraction of the total anomalies (44%) is formed during the last year before the parcels reach the coast (Figure 9b), and the difference between $CHL_{0.05}$ and CHL_{clim} is due at first order to a difference in subsurface heating by the radiative forcing. However, some differences with the Benguela upwelling appear. First the warming due to mixing is larger in the Senegal-Mauritania upwelling (Figures 9f and 9h), suggesting that turbulent processes are more active in this upwelling. Second the pathways are much more similar between CHL_{clim} and $CHL_{0.05}$ (Figures 8e, 8f, 8g, and 8h) than in the Benguela, suggesting that the dynamics of the Senegal-Mauritania upwelling system is less impacted by the biology.

6. Summary and Discussion

We investigated the impact of the biologically modulated absorption of solar radiation on the physics of the Tropical Atlantic Ocean with a special focus on the Benguela and Mauritania-Senegal upwelling systems. Experiments with time and spatially varying concentrations of surface chlorophyll (obtained from satellite ocean color observations) were performed and compared to an experiment forced with constant chlorophyll concentration set to 0.05 mg m^{-3}, representative of chlorophyll depleted waters. Comparison with observations shows that the reference simulation ($CHL_{0.05}$) realistically represents the ocean background state and its seasonal variability. Taking into account realistic chlorophyll concentrations leads to a significant cooling of the sea surface in the upwelling regions, reaching ~ -1°C in the Benguela and Mauritania-Senegal upwellings.

This cooling is in agreement with previous studies performed in the Pacific [*Nakamoto et al*., 2001; *Manizza et al*., 2005; *Lin et al*., 2007, 2008; *Frouin et al*., 2007; *Anderson et al*., 2009; *Park et al*., 2014a,2014b] but in contradiction with others that show a warming of the coastal and equatorial upwelling systems [*Timmermann and Jin*, 2002; *Murtuggude et al*., 2002; *Marzeion et al*., 2005; *Wetzzel et al*., 2006; *Lengaigne et al*., 2007]. In the Atlantic, *Frouin et al*. [2007] performed sensitivity experiments that are relatively similar to ours. They also found a cooling of the eastern boundary upwelling of the same order of us (around 1°C). Since the absolute values of the observed cooling depend on the reference used, our study focuses on the processes involved rather than on the absolute evolution of the SST.

The processes responsible for the observed cooling are identified analyzing backward the properties (temperature, depth) and heat budget of the upwelled waters. Although the currents and the mixed-layer depth are modified between the two simulations (as observed in other studies; e.g., *Frouin et al*. [2007]), our results suggest that changes in the dynamics of the upwelling (i.e., modification of horizontal, vertical advection, and vertical mixing) do not explain at first order the SST response in the Benguela and Mauritania-Senegal upwellings. Instead, the cooling anomalies observed in the upwelling regions mainly reflect the deficit of heating of subsurface waters due to the chlorophyll absorption of heat at the surface along their transit to

the upwelling cell. This contrasts with previous studies in other upwelling regions which proposed that dynamical modifications of the upwelling are responsible for the observed temperature anomalies [*Manizza et al*. 2005; *Marzeoin et al*., 2005; *Nakamoto et al*., 2001; *Loptien et al*., 2009; *Sweeney et al*., 2005; *Lengaigne et al*., 2007; *Lin et al*., 2007, 2008; *Park et al*., 2014a,2014b].

We focused on the two main coastal upwellings of the Tropical Atlantic (the Benguela and Mauritania Senegal upwellings). However, we also found a weak cooling (∼0.5°C) in the equatorial Atlantic upwelling. It would be interesting to further understand the details of the mechanisms responsible for this cooling, and to explain in contrast to the Pacific Ocean, where the largest sensitivity of the SST to the biology is generally found at the equator [e.g., *Park et al*., 2014b], the largest sensitivity in the Tropical Atlantic is found within the upwelling systems. This could be the focus of a subsequent study.

The upper ocean heat content of the eastern Tropical Atlantic is strongly affected by the heat storage due to the chlorophyll absorption. There is a close match between the distribution of the temperature anomalies below the mixed-layer (Figure 4e) and ML distribution (Figures 3b and 3d). This illustrates that the impact of the chlorophyll is important where the mixed-layer depth is shallow. As expected, a deep mixed-layer absorbs and homogenizes almost the entire fraction of solar radiation while a shallow mixed-layer allows (i) a larger fraction of solar radiation to penetrate below the mixed-layer base, and (ii) the persistence of the differential heating owing to generally weak mixing between the ML and the waters below. This corroborates previous results of *Ma et al*. [2012, 2014] who found weak SST changes in winter in the Arabian Sea and the South China Sea in the presence of a thick and chlorophyll-rich ML.

Our study suggests that 43.8% (∼23%) of the temperature anomaly in the Benguela (Senegal-Mauritania upwelling) is due to the initial difference 4 years backwards. Differences in the mean depth of the water parcels between the two simulations suggest that these anomalies are due to differences in the advection pathways. Nevertheless, we cannot completely discard that these anomalies could be due to differential heating (or even mixing) affecting the waters before year 4, the time limit of our backward integration. Despite this uncertainty, we could diagnose that the largest part (56.2% for the Benguela upwelling, 77.3% for the Senegal-Mauritania upwelling) of the anomalies form during the 4 years prior to the entrance to the upwelling, the main cause being differential heating. We found that 64% of the final temperature anomaly between the two simulations is generated in regions with surface chlorophyll concentration higher than 1 mg m^{-3} while the remaining 36% of the anomaly is created in regions with surface chlorophyll concentration lower than 1 mg m^{-3}. This result echoes results of *Anderson et al*. [2009] who analyzed the sensitivity of the Pacific equatorial temperature to chlorophyll concentrations and found that the chlorophyll off equator, in near-oligotrophic regions, play a key role on the sensitivity of the equatorial temperatures.

The impact of the seasonal variability of the chlorophyll concentrations has been investigated using an additional simulation with mean chlorophyll concentrations. The results suggest that the temporal variability of the chlorophyll has not a significant effect on the seasonal variability of the surface temperature anomalies. As shown in Figure 12f, the seasonality of the subsurface heating rate is at first order modulated by the seasonal cycle of the shortwave radiation (Figure 11c) and not by the variability of the chlorophyll concentrations.

It is important to note that the model is forced at the surface using bulk formulae that damp the sensitivity to surface chlorophyll. This is highlighted by the positive anomalies of net air-sea fluxes (+20 W m^{-2} in the upwelling areas), that act to reduce the temperature anomalies. It is not clear to which extent this damping limits the surface cooling and modifies the large scale mean state. This is the main drawback of a forced-ocean modeling approach. Our guess is that the main processes identified in this study may still be relevant in a coupled framework, however this definitely would require verification using coupled ocean-atmosphere simulations.

In addition, the use of a forced ocean model did not allow to take into account potential atmospheric feedbacks on the ocean response. In the Tropical Pacific, substantial differences in the sensitivity to biology are observed when atmospheric feedbacks are allowed or not [e.g., *Lengaigne et al*., 2007 or *Loptien et al*., 2011]. Even with a coupled ocean model, conflicting results are obtained when including the biological effect: *Park et al*. [2014a,2014b] shows that SST cooling is amplified in the fully coupled model (ocean-atmosphere-biogeochemistry) experiments whereas *Marzeion et al*. [2005] or *Lengaigne et al*. [2007] found a warming with an hybrid coupled model or a fully coupled-model, respectively. In the case of the Benguela and the Mauritania-Senegal upwelling systems, no studies have been performed with a coupled ocean model. We can hypothesize that the biological effect may trigger a negative feedback in coastal upwelling

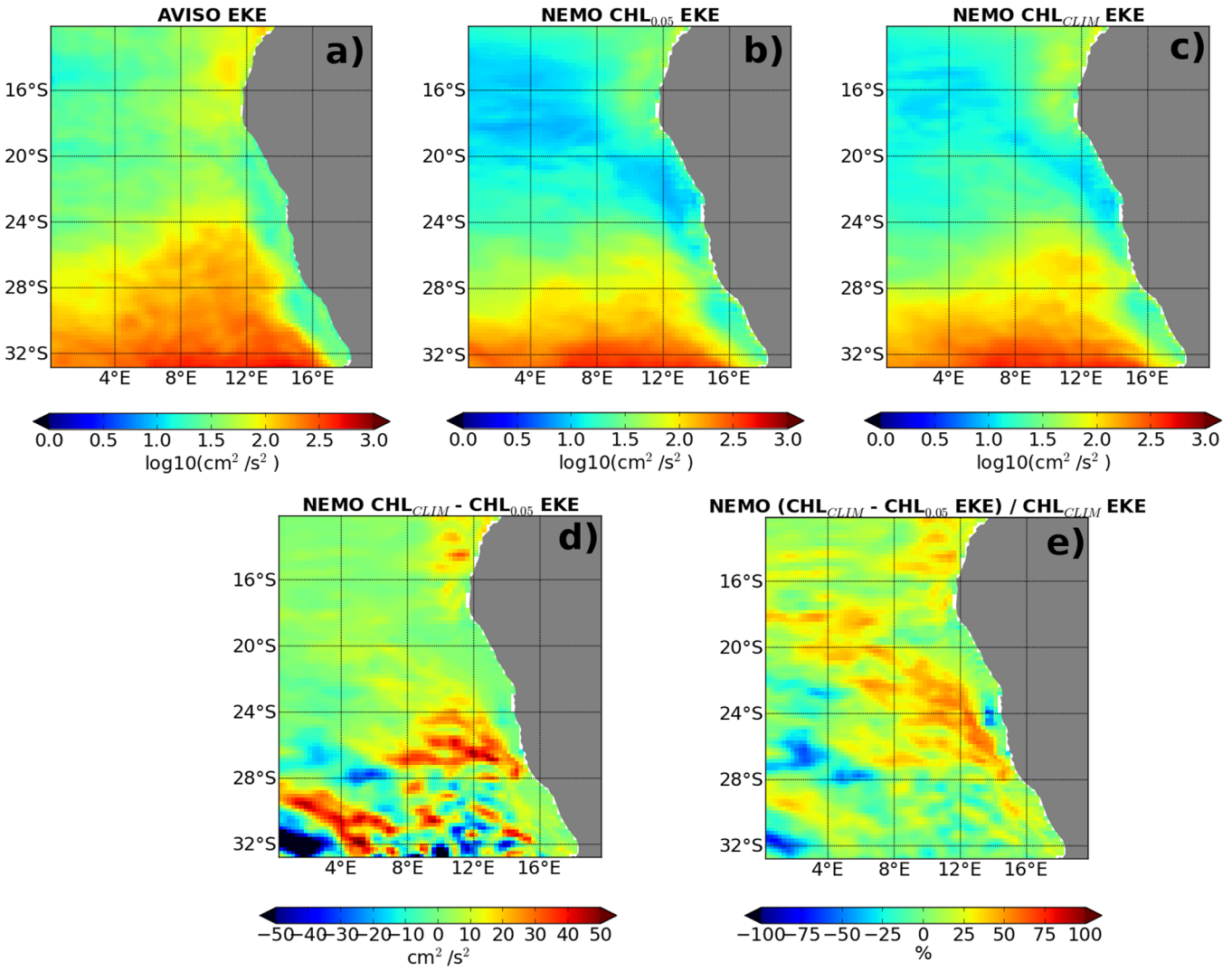

Figure 13. Mean eddy kinetic energy (EKE) for the period 2005–2012 from (a) AVISO observations (log10 $cm^2\ s^{-2}$), (b) $CHL_{0.05}$ simulation (log10 $cm^2\ s^{-2}$), (c) CHL_{clim} simulation (log10 $cm^2\ s^{-2}$), (d) difference of EKE between CHL_{clim} and $CHL_{0.05}$ ($cm^2\ s^{-2}$), (e) difference of EKE in %. The EKE is computed from geostrophic velocity anomalies as $(1/2)(u'^2 + v'^2)$, where u′ is a model or altimetry velocity anomaly with respect to the mean seasonal cycle.

systems: a nearshore cooling may induce a decrease in upwelling-favorable wind stress due to the enhanced boundary layer stratification [*Small et al*., 2008; *Chelton et al*., 2007], which may in turn reduce the upwelling and thus the surface cooling. We should also expect a positive air-sea feedback in equatorial upwelling regions due to modifications of the Walker circulation when taking into a ocean-atmosphere coupled model, which would amplify the observed cooling anomalies. Thus, the response to the differential heating should be further investigated in such complex dynamical systems.

Our forcing strategy makes use of remote sensing chlorophyll concentrations. Chlorophyll concentration is characterized by a pronounced variability which strongly depends of the ocean circulation and the water masses structure, so the concentrations obtained by remote sensing are not necessarily coherent with the physical fields computed by the model. Using a biogeochemical model may solve this issue. Nevertheless, state of the art, physical-biogeochemical models still shows substantial biases in representing the distribution of chlorophyll concentrations in the upwelling areas [e.g., *Aumont et al*., 2015]. We do think that the impact of these biases on our results would largely overcome the errors due to a possible inconsistency between the physics and the concentrations obtained by remote sensing.

In addition to the profound consequences it has on the ocean mean state, the biological differential heating has a significant and indirect impact on the eddy field. This has been evidenced by *Loptien et al*. [2009] who

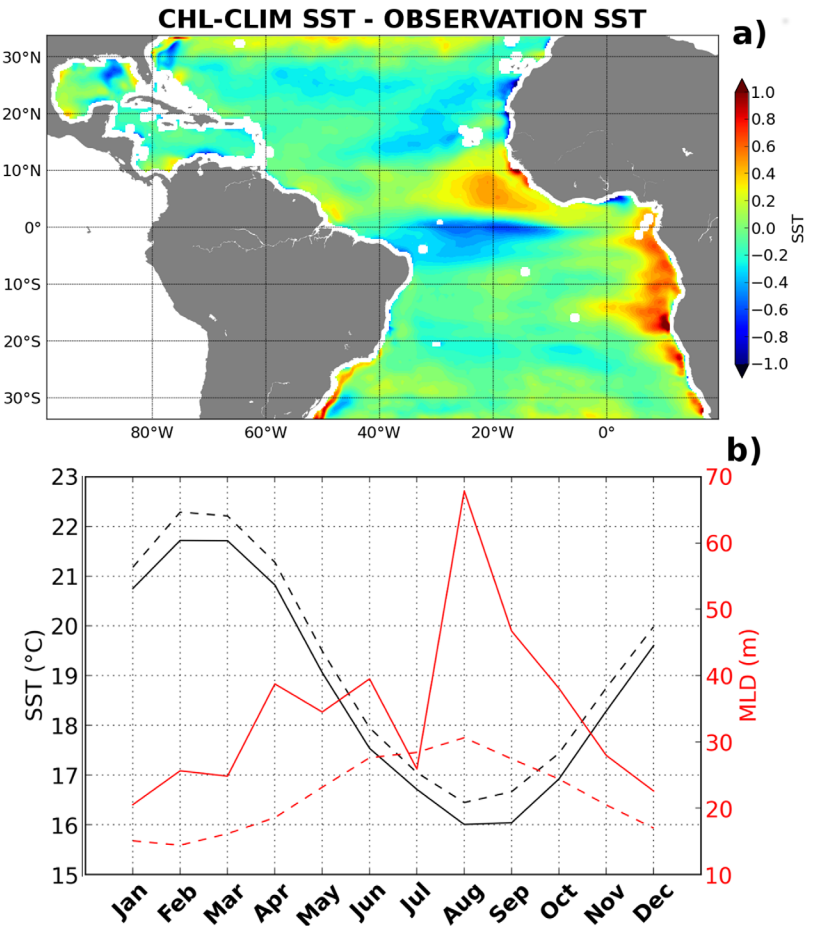

Figure 14. (a) Annual mean SST difference between CHL_{clim} and OI microwave observations (°C). (b) Mean seasonal cycle of SST (black; °C) and MLD (red; meters) for the Benguela and Senegal region (as defined in Figure 1) for the model (dotted line) and observations (continuous line).

found a 100% increase of the eddy kinetic energy (EKE) associated with a surface cooling in the equatorial Pacific when including the biological feedback. They explained this response by an intensification of the equatorial currents and associated horizontal and vertical shear. Interestingly, we also observed an EKE increase in the Atlantic Ocean at the equator and in the eastern boundary upwellings. This increase is particularly marked in the Benguela upwelling (Figure 13), with values 40% larger offshore of the upwelling (Figure 13e). The inclusion of the biological effect reduces the gap between the modeled EKE (Figure 13c) and the EKE inferred from altimetry (Figure 13a). The eddies in upwelling systems are known to play a key role on the cross-shore heat balance [e.g., *Colas et al*., 2011; *Jouanno and Sheinbaum*, 2013], so that these modifications associated with the biological effect may impact the heat budget of the upwelling system, particularly the offshore eddy-associated transport of temperature anomalies. Owing to the relatively low horizontal resolution of our (eddy-permitting) model, we did not estimate the contribution of the mean currents changes versus the contribution of the eddies changes induced by the biology. Such a study would be more pertinent if it were addressed using an eddy-resolving model.

Our regional approach has the advantage of a controlled framework, which allows to disentangle local and regional processes avoiding complications due to global scale or remote response. However, one main caveat is that the Benguela and Mauritania-Senegal upwellings are located near the boundaries of our domain, with a substantial fraction of the upwelled waters that are advected from the boundaries. Nevertheless, we do not think that this invalidates our conclusions regarding the processes involved in the response of these upwellings to biological differential heating. Indeed: (i) a large fraction of the temperature anomaly forms near the upwelling during the last year that precedes the upwelling of the water parcels, (ii) half of the upwelling source waters originate from the equatorial region, (iii) the boundary conditions are the same for all the simulations so they cannot be the source of the diagnosed temperature anomalies.

Overall, our results suggest that the vertical modulation of the penetration of the solar radiation is a key parameter of the tropical climate. Inclusion of the biological feedback contributes to reduce the strong warm bias observed along the Benguela upwelling (Figures 3 and 14) and reported in most of the CMIP5 models [*Taylor et al*., 2012; *Richter et al*., 2012; *Wang et al*., 2014]. Indeed the 1°C warm bias in the Benguela upwelling is reduced to 0.5°C in the upwelling area from 20°S to 27°S (Figure 14). Thus, taking into account the effect of the chlorophyll improves the representation of the Benguela upwelling SST, but we should note however that it also increases a subsurface cold bias below the mixed-layer (not shown). Such response was also observed by *Ma et al*. [2014] in the Arabian Sea. The surface temperature cold bias in the equatorial region from 10°S to 10°N is also moderately amplified when including the chlorophyll effect in our simulations. Ultimately, these results point out the importance that should be granted to a correct representation of the vertical penetration of the radiative forcing in the ocean.

Appendix A

The impact of using i) a variable chlorophyll profile (following the formulation of *Morel and Berthon* [1989]) or ii) a constant chlorophyll profile has been tested by comparing two long term simulations (1979–2012). As shown in Figure A1, the difference of surface temperature between the two cases is lower than 0.2°C. This difference is considered as weak compared to the 1.4°C sea surface temperature difference between the simulations CHL0.05 and CHLclim.

The evolution of the temperature anomalies in the upper 200m illustrates the time required for the basin scale upper ocean temperature to equilibrate in response to the modification of the chlorophyll concentrations (Figure A2).

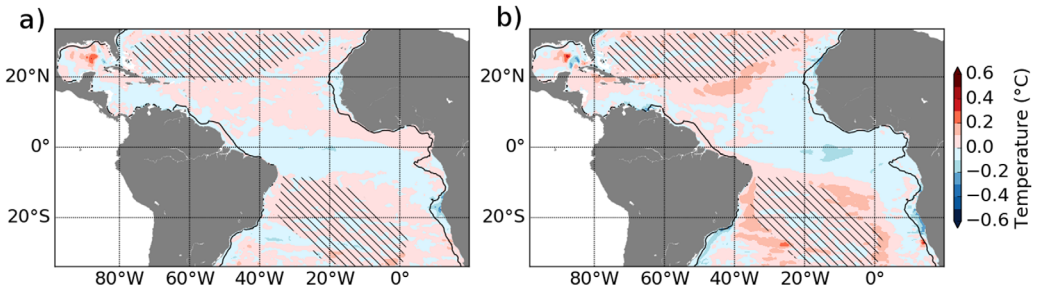

Figure A1. SST difference between simulations performed with the chlorophyll profile parameterization from *Morel and Berthon* [1989] (as in the remaining of the manuscript) and simulations performed with a constant chlorophyll profile, for both (a) CHL0.05 and (b) CHLclim cases.

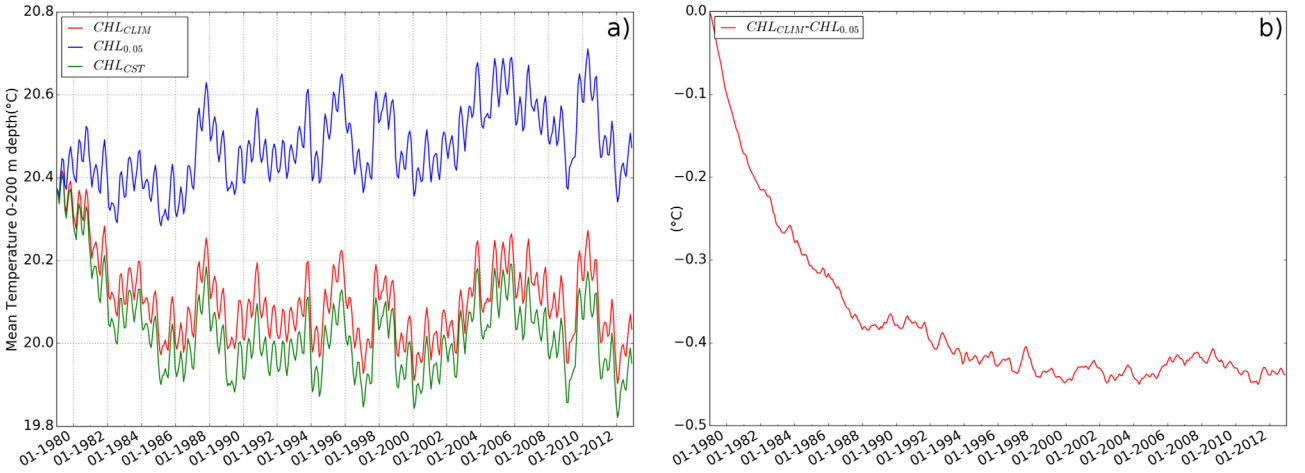

Figure A2. (a) Monthly mean temperature averaged over the entire domain between the surface and 200 m depth. (b) Difference between CHLclim and CHL 0.05.

Acknowledgments
This study was supported by EU FP7/2007–2013 under grant 603521, project PREFACE. Model outputs are freely available on request. Computing facilities were provided by GENCI project GEN7298. GlobColour data (http://globcolour.info) used in this study has been developed, validated, and distributed by ACRI-ST, France. Thanks to B. Blanke and N. Grima for making available the ARIANE Lagrangian tool (http://www.univ-brest.fr/lpo/ariane/). We acknowledge discussion with B. Bourles. The altimeter products were produced by SSALTO-DUACS and distributed by AVISO with support from CNES (http://www.aviso.oceanobs.com/duacs/). We thank two anonymous reviewers for their constructive remarks.

References

Anderson, W. G., A. Gnanadesikan, and A. Wittenberg (2009), Regional impacts of ocean color on tropical Pacific variability, *Ocean Sci. Discuss.*, *6*(1), 243–275.
Aumont, O., C. Ethé, A. Tagliabue, L. Bopp, and M. Gehlen (2015), PISCES-v2: An ocean biogeochemical model for carbon and ecosystem studies, *Geosci. Model Dev.*, *8*(8), 2465–2513.
Blanke, B., and S. Raynaud (1997), Kinematics of the Pacific Equatorial Undercurrent: An Eulerian and Lagrangian approach from GCM results, *J. Phys. Oceanogr.*, *27*, 1038–1053, doi:10.1175/1520-0485(1997)027.
Blanke, B., M. Arhan, G. Madec, and S. Roche (1999), Warm water paths in the equatorial Atlantic as diagnosed with a general circulation model, *J. Phys. Oceanogr.*, *29*, 2753–2768, doi:10.1175/1520-0485(1999)029.
Brodeau, L., B. Barnier, A.-M. Treguier, T. Penduff, and S. Gulev (2010), An ERA40-based atmospheric forcing for global ocean circulation models, *Ocean Modell.*, *31*(3–4), 88–104.
Chelton, D. B., M. G. Schlax, and R. M. Samelson (2007), Summertime coupling between sea surface temperature and wind stress in the California Current System, *J. Phys. Oceanogr.*, *37*, 495–517, doi:10.1175/JPO3025.1.
Colas, F., J. C. McWilliams, X. Capet, and J. Kurian (2011), Heat balance and eddies in the Peru–Chile current system, *Clim. Dyn.*, *39*, 509–529, doi:10.1007/s00382-011-1170-6.
Cury, P., and L. Shannon (2004), Regime shifts in the Benguela ecosystem: Facts, theories and hypotheses, *Prog. Oceanogr.*, *60*, 223–243, doi:10.1016/j.pocean.2004.02.007.
Cropper, T. E., E. Hanna, and G. R. Bigg, (2014), Spatial and temporal seasonal trends in coastal upwelling off Northwest Africa, 1981–2012, *Deep Sea Res., Part II*, *86*, 94–111.
de Boyer Montégut, C., G. Madec, A. S. Fischer, A. Lazar, and D. Iudicone (2004), Mixed layer depth over the global ocean: An examination of profile data and a profile-based climatology, *J. Geophys. Res.*, *109*, C12003, doi:10.1029/2004JC002378.
de Boyer Montégut, C., J. Vialard, S. S. C. Shenoi, D. Shankar, F. Durand, C. Ethé, and G. Madec (2007), Simulated seasonal and interannual variability of mixed layer heat budget in the northern Indian Ocean, *J. Clim.*, *20*, 3249–3268, doi:10.1175/JCLI4148.1.
Dee, D. P., et al. (2011), The ERA-Interim reanalysis: Configuration and performance of the data assimilation system, *Q. J. R. Meteorol. Soc.*, *137*, 553–597, doi:10.1002/qj.828.
Dussin, R., B. Barnier, and L. Brodeau (2014), The making of Drakkar forcing set DFS5, *DRAKKAR/MyOcean Rep. 05–10-14*, Lab. de Glaciol. et Géophys. de l'Environ., Grenoble, France.
Duteil, O., A. Lazar, Y. Dandonneau, I. Wainer, and C. Menkes (2009), Deep chlorophyll maximum and upper ocean structure interactions: Case of the Guinea Thermal Dome, *J. Mar. Res.*, *67*(2), 239–271, doi:10.1357/002224009789051191.
Fanton d'Andon, O., A. Mangin, S. Lavender, D. Antoine, S. Maritorena, A. Morel, and G. Barrot (2009), GlobColour—The European Service for Ocean Colour, in *Proceedings of the 2009 IEEE International Geoscience & Remote Sensing Symposium*, *12–17 July 2009*, IEEE Geosci. and Remote Sens. Soc., Cape Town, South Africa. [Available at https://espace.curtin.edu.au/handle/20.500.11937/42230.]
Fischer, G., O. Romero, U. Merkel, B. Donner, M. Iversen, N. Nowald, V. Ratmeyer, G. Ruhland, M. Klann, and G. Wefer (2016), Deep ocean mass fluxes in the coastal upwelling off Mauritania from 1988 to 2012: Variability on seasonal to decadal timescales, *Biogeosciences*, *13*, 3071–3090, doi:10.5194/bg-13-3071-2016.
Frouin, R., K. Ueyoshi, and M. Kampel (2007), Influence of solar radiation absorbed by phytoplankton on the thermal structure and circulation of the tropical Atlantic Ocean, in *Proceedings of SPIE, Coastal Ocean Remote Sens.*, vol. 6680, edited by R. J. Frouin, Coastal Ocean Remote Sensing, San Diego, Calif., doi:10.1117/12.738969.
Hernandez, O., J. Jouanno, and F. Durand (2016), Do the Amazon and Orinoco freshwater plumes really matter for hurricane-induced ocean surface cooling?, *J. Geophys. Res. Oceans*, *121*, 2119–2141, doi:10.1002/2015JC011021
Jouanno, J., and J. Sheinbaum (2013), Heat balance and eddies in the Caribbean upwelling system, *J. Phys. Oceanogr.*, *43*(5), 1004–1014.
Jouanno, J., F. Marin, Y. du Penhoat, J. Sheinbaum, and J.-M. Molines (2011a), Seasonal heat balance in the upper 100 m of the equatorial Atlantic Ocean, *J. Geophys. Res.*, *116*, C09003, doi:10.1029/2010JC006912.
Jouanno, J., F. Marin, Y. du Penhoat, J.-M. Molines, and J. Sheinbaum (2011b), Seasonal modes of surface cooling in the Gulf of Guinea, *J. Phys. Oceanogr.*, *41*(7), 1408–1416, doi:10.1175/JPO-D-11-031.1.
Large, W. G., and S. Yeager, (2009), The global climatology of an interannually varying air-sea ux data set, *Clim. Dyn.*, *33*, 341–364, doi: 10.1007/s00382-008-0441-3.
Lengaigne, M., et al. (2007), Influence of the oceanic biology on the tropical Pacific climate in a coupled general circulation model, *Clim. Dyn.*, *28*, 503–516.
Lin, P., H. Liu, and X. Zhang (2007), Sensitivity of the upper ocean temperature and circulation in the equatorial pacific to solar radiation penetration due to phytoplankton, *Adv. Atmos. Sci.*, *24*(5), 765–780.
Lin, P., H. Liu, and X. Zhang (2008), Effect of chlorophyll-a spatial distribution on upper ocean temperature in the central and eastern equatorial Pacific, *Adv. Atmos. Sci.*, *25*(4), 585–596.
Lin, P., H. Liu, Y. Yu, and X. Zhang (2011), Response of sea surface temperature to chlorophyll-a concentration in the tropical Pacific: Annual mean, seasonal cycle, and interannual variability, *Adv. Atmos. Sci.*, *28*(3), 492–510.
Loptien, U., C. Eden, A. Timmermann, and H. Dietze (2009), Effects of biologically induced differential heating in an eddy-permitting coupled ocean-ecosystem model, *J. Geophys. Res.*, *114*, C06011, doi:10.1029/2008JC004936.
Ma, J., H. Liu, H. Zhan, P. Lin, and Y. Du (2012), Effects of chlorophyll on upper ocean temperature and circulation in the upwelling regions of the South China Sea, *Aquat. Ecosyst. Health Manage.*, *15*(2), 127–134, doi:10.1080/14634988.2012.687663.
Ma, J., H. Liu, P. Lin, and H. Zhan (2014), Seasonality of biological feedbacks on sea surface temperature variations in the Arabian Sea: The role of mixing and upwelling, *J. Geophys. Res. Oceans*, *119*, 7592–7604, doi:10.1002/2014JC010186 .
Madec, G. (2014), *"NEMO ocean engine" (Draft edition r5171). Note du Pôle de modélisation*, No. 27, Inst. Pierre-Simon Laplace, France, 1288–1619.
Manizza, M., C. Le Quere, A. J. Watson, and E. T. Buitenhuis (2005), Biooptical feedbacks among phytoplankton, upper ocean physics and sea-ice in a global model, *Geophys. Res. Lett.*, *32*, L05603, doi:10.1029/2004GL020778.
Maritorena S., O. H. Fanton d'Andon, A. Mangin, and D. A. Siegel (2010), Merged satellite ocean color data products using a bio-optical model: Characteristics, benefits and issues, *Remote Sens. Environ.*, *114*, 1791–1804.
Marzeion, B., A. Timmermann, R. Murtuggude, and F. F. Jin (2005), Biophysical feedbacks in the Tropical Pacific, *J. Clim.*, *18*, 58–70.
Morel, A. (1988), Optical modeling of the upper ocean in relation to its biogenous matter content, *J. Geophys. Res.*, *93*, 10,749–10,768.
Morel, A., and J. F. Berthon (1989), Surface pigments, algal biomass profiles, and potential production of the euphotic layer: Relationships reinvestigated in view of remote-sensing applications, *Limnol. Oceanogr.*, *34*, 1545–1562.

Murtugudde, R., J. Beauchamp, and A. Busalacchi (2002), Effects of penetrative radiation in the upper ocean tropical ocean circulation, *J. Clim.*, *15*, 470–486.

Nakamoto, S., S. Prasanna Kumar, J. Oberhuber, J. Ishizaka, K. Muneyama, and R. Frouin (2001), Response of the equatorial Pacific to chlorophyll pigment in a mixed-layer isopycnal ocean general circulation model, *Geophys. Res. Lett.*, *28*, 2021–2024.

Newinger, C., and R. Toumi (2015), Potential impact of the colored Amazon and Orinoco plume on tropical cyclone intensity, *J. Geophys. Res. Oceans*, *120*, 1296–1317, doi:10.1002/2014JC010533.

Park, J.-Y., J.-S. Kug, and Y.-G. Park (2014a), An exploratory modeling study on bio-physical processes associated with ENSO, *Prog. Oceanogr.*, *124*, 28–41.

Park, J.-Y., J.-S. Kug, H. Seo, and J. Bader (2014b), Impact of bio-physical feedbacks on the tropical climate in coupled and uncoupled GCMs, *Clim. Dyn.*, *43*, 1811–1827

Reffray, G., R. Bourdalle-Badie, and C. Calone (2015), Modelling turbulent vertical mixing sensitivity using a 1-D version of NEMO, *Geosci. Model Dev.*, *8*, 69–86, doi:10.5194/gmd-8-69-2015.

Renault, L., B. Dewitte, P. Marchesiello, S. Illig, V. Echevin, G. Cambon, M Ramos, O. Astudillo, P. Minis, and J. K. Ayers (2012), Upwelling response to atmospheric coastal jets off central Chile: A modeling study of the October 2000 event, *J. Geophys. Res.*, *117*, C02030, doi: 10.1029/2011JC007446.

Reverdin, G., E. Kestenare, C. Frankignoul, and T. Delcroix (2007), Surface salinity in the Atlantic Ocean (30°S–50°N), *Prog. Oceanogr.*, *73*, 311–340, doi:10.1016/j.pocean.2006.11.004.

Richter, I., S.-P. Xie, S. K. Behera, T. Doi, and Y. Masumoto (2012), Equatorial Atlantic variability and its relation to mean state biases in CMIP5, *Clim. Dyn.*, *42*, 171–188, doi:10.1007/s00382-012-1624-5.

Signorini, S. R., R. G. Murtugudde, C. R. McClain, J. R. Christian, J. Picaut, and A. J. Busalacchi (1999), Biological and physical signatures in the tropical and subtropical Atlantic, *J. Geophys. Res.*, *104*, 18,367–18,382, doi:10.1029/1999JC900134.

Small, R., S. deSzoeke, S. Xie,L. O'Neill, H. Seo, Q. Song, P. Cornillon, M. Spall, and S. Minobe (2008), Air–sea interaction over ocean fronts and eddies, *Dyn. Atmos. Oceans*, *45*, 274–319, doi:10.1016/j.dynatmoce.2008.01.001.

Sweeney, C., A. Gnanadesikan, S. M. Griffies, M. J. Harrison, A. J. Rosati, and B. L. Samuels (2005), Impacts of shortwave penetration depth on large-scale ocean circulation and heat transport, *J. Phys. Oceanogr.*, *35*(6), 1103–1119.

Taylor, K. E., R. J. Stouffer, and G. A. Meehl (2012), An overview of CMIP5 and the experiment design, *Bull. Am. Meteorol. Soc.*, *93*, 485–498.

Timmermann A., and F. F. Jin (2002), Phytoplankton influences on tropical climate, *Geophys. Res. Lett.*, *26*(23), doi:10.1175/jpo2740.1.

Wetzel P., E. Maier-Reimer, M. Botzet, J. Jungclaus, N. Keenlyside, and M. Latif (2006), Effects of ocean biology on the penetrative radiation in a coupled climated model, *J. Clim.*, *19* (16), 373–3987 , doi:10.1175/jcli3828.1.

Wang, C., L. Zhang, S.-K. Lee, L. Wu, and C. R. Mechoso (2014), A global perspective on CMIP5 climate model biases, *Nat. Clim. Change*, *4*, 201–205, doi:10.1038/nclimate2118.